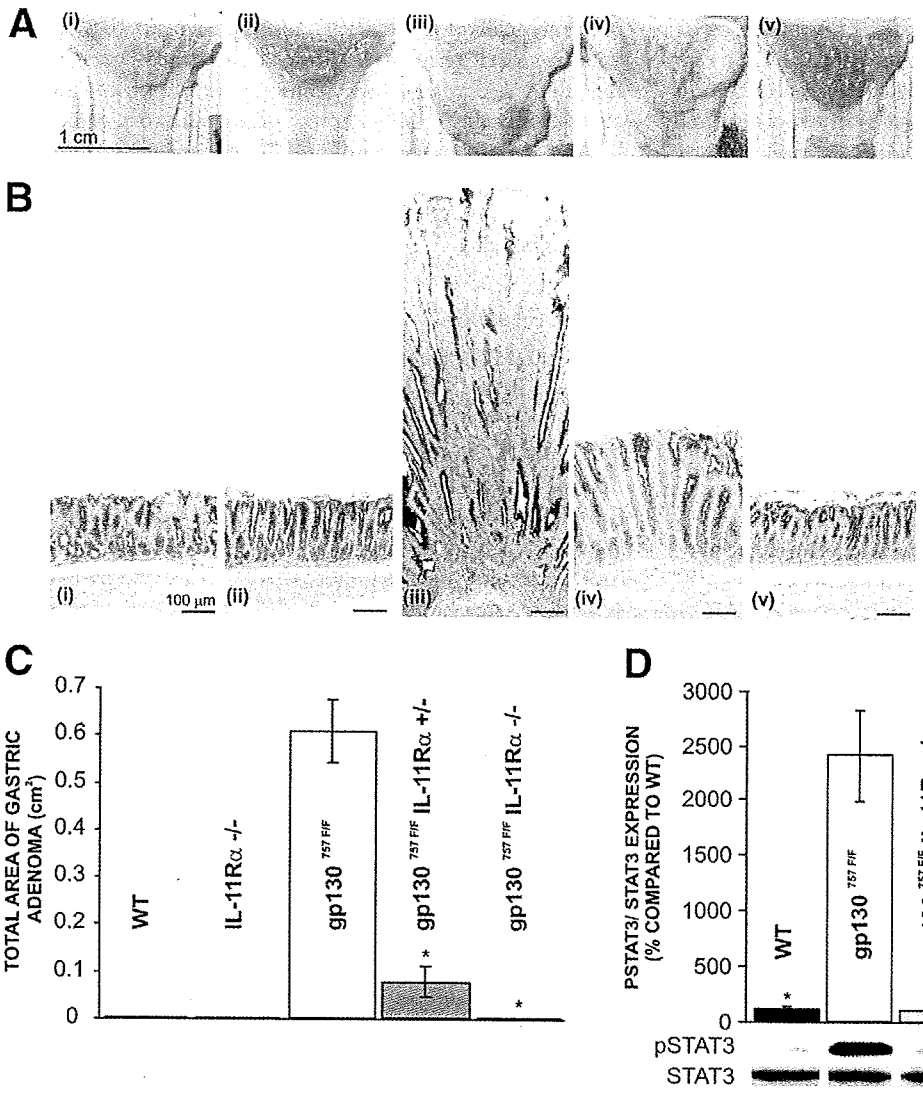

Figure 2. (*A*) Macroscopic and (*B*) Alcian blue/periodic acid–Schiff–stained microscopic images of WT (i), IL-11Rα-/- (ii), gp130$^{757F/F}$ (iii), gp130$^{757F/F}$IL-11Rα+/- (iv), and gp130$^{757F/F}$IL-11Rα-/- (v) stomachs. (*C*) Tumor area (cm^2) was measured from macroscopic images. (*D*) Ratio of pSTAT3:STAT3 was measured in antral stomach. *$P < .05$ compared with gp130$^{757F/F}$. *Scale bar*, 100 μm.

IL-11Rα Signaling Is Crucial for Tumorigenesis in gp130$^{757F/F}$ Mice

WT, IL-11Rα-/-, gp130$^{757F/F}$, gp130$^{757F/F}$IL-11Rα+/-, and gp130$^{757F/F}$IL-11Rα-/- mice were analyzed for gastric tumorigenesis (Figure 2*A*i–v). A proportion of gp130$^{757F/F}$ IL-11Rα+/- (2 of 5) did not develop tumors and those that did were smaller macroscopically (Figure 2*A*iv), microscopically (Figure 2*B*iv), and when quantified (Figure 2*C*). Furthermore, tumors were completely ablated in gp130$^{757F/F}$IL-11Rα-/- mice (Figure 2*A*, *B*v, and *C*), a finding replicated independently by Ernst et al.[22] This shows that IL-11 signaling is absolutely required for gp130$^{757F/F}$ tumorigenesis.

We show that IL-11Rα signaling is exclusively responsible for increased p-STAT3 in gp130$^{757F/F}$ antrum, causal of gp130$^{757F/F}$ tumors,[15] because p-STAT3 is at WT levels in gp130$^{757F/F}$IL-11Rα-/- antrum (Figure 2*D*). Thus, signaling via IL-11 is crucial for hyper-p-STAT3, correlating with antral tumor development in gp130$^{757F/F}$ mice.

Fundic Hyperplasia Is Reduced in HK-β-/-IL-11Rα-/- Mice Irrespective of Gastrin Expression

HK-β-/- mice develop gastrin-dependent gross fundic hyperplasia[23] (Figure 3*A* and *B*ii). To determine the contribution of IL-11 to pathology, HKβ-/-IL-11Rα-/- mice were analyzed. HKβ-/-IL-11Rα-/- mice had significantly reduced fundic hyperplasia macroscopically (Figure 3*A*iii), microscopically (Figure 3*B*iii), and when quantified (Figure 3*C*). To determine if altered gastrin expression contributed to the reduced hyperplasia, gastrin-expressing G cells were stained immunohistochemically (Figure 3*D*i–iii). G cells were equally increased in HKβ-/- and HKβ-/-IL-11Rα-/- compared with WT mice (Figure 3*E*), as was gastrin mRNA by quantitative PCR (Figure 3*F*), showing the reduced hyperplasia in HKβ-/-IL-11Rα-/- mice was not caused by altered gastrin. Somatostatin, the negative regulator of gastrin, also was quantified by quantitative PCR and was

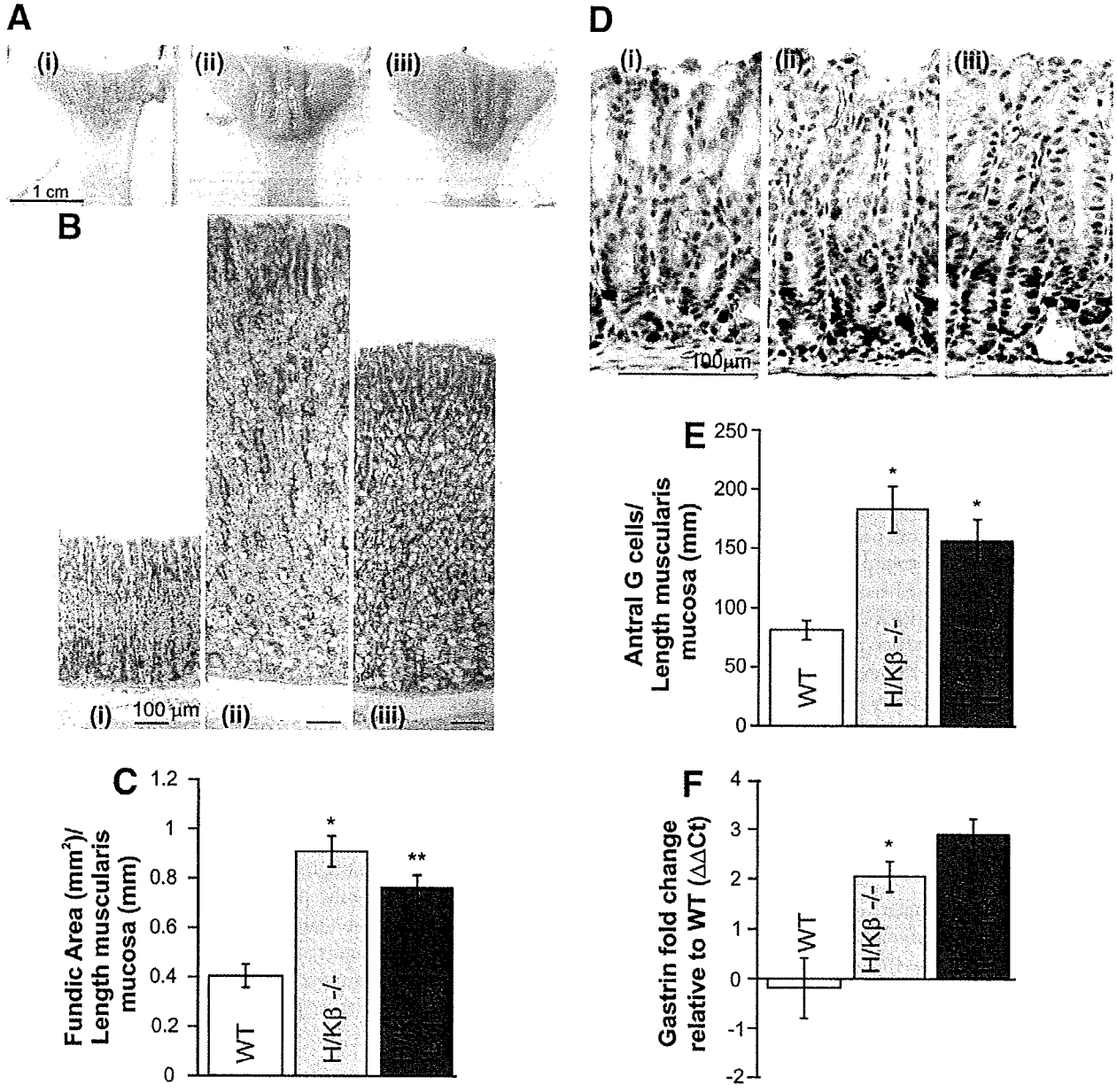

Figure 3. (*A*) Macroscopic and (*B*) H&E-stained microscopic images of fundus from WT (i), HKβ-/- (ii), and HKβ-/-IL-11Rα-/- (iii) mice. (*C*) Fundic area (mm^2) was measured (n ≥ 12/genotype) from digital images and standardized against muscularis mucosal length (mm). (*D*) Gastrin-expressing G cells were localized immunohistochemically in WT (i), HKβ-/- (ii), and HKβ-/-IL-11Rα-/- (iii) antrum, counted by light microscopy (n ≥ 5/genotype), and (*E*) standardized against muscularis mucosal length (mm). (*F*) Gastrin mRNA was quantified by quantitative PCR, standardized to housekeeper L32, and expressed as fold change over WT (ΔΔCt). Scale bars, 1 cm and 100 μm as marked. *$P < .05$ compared with WT. **$P < .05$ compared with all groups.

equivalent in WT, HKβ-/-, and HKβ-/-IL-11Rα-/- mice (data not shown). This illustrates that IL-11 can drive gastric pathology, irrespective of a gp130 mutation or hypergastrinemia.

WT Gastric Antral Mucosa Is Biased Toward a p-STAT3 Response When Stimulated With IL-11 But Not IL-6

We examined the effect of a single IL-11 dose (5 μg IP) on WT stomach and compared this with a single IL-6 dose (5 μg IP). IL-11 administration caused a 4.4-fold (±0.77; n = 5; $P < .05$) increase in p-STAT3 in antral mucosa with no effect on p-ERK1/2 (Figure 4*A*). In contrast, IL-6 did not induce a p-STAT3 or p-ERK 1/2 response in the antrum (Figure 4*A*), despite antral IL-6Rα mRNA (data not shown), and p-STAT3 activation by IL-6 in liver (data not shown). This shows that IL-11 (not IL-6) administration can mimic the unbalanced gp130 signaling seen in $gp130^{757F/F}$ antral tumors, hyperactivation of p-STAT3 but no p-ERK1/2 induction.

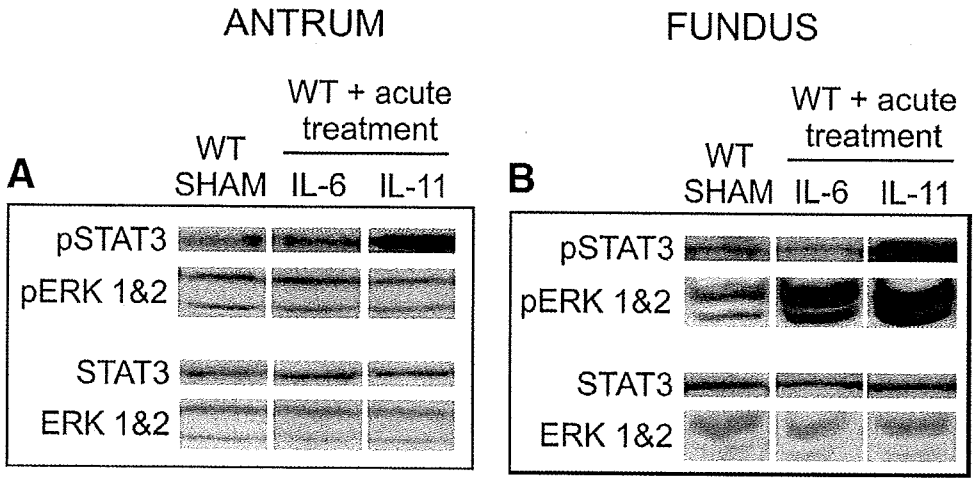

Figure 4. STAT3, p-STAT3, ERK 1/2, and p-ERK 1/2 were measured in the (*A*) antral and (*B*) fundic stomach of WT mice after IP administration of 5 μg IL-6, IL-11, or saline (sham). Representative bands from each group are shown (n ≥ 7).

In gp130$^{757F/F}$ mice, tumors initiate in the antrum and at early stages the fundus is tumor free.[14] We examined signaling outputs in fundus compared with antrum of cytokine-treated mice. In WT fundus, IL-11 administration caused increased p-STAT3 (8.8-fold ± 1.8; $P < .05$) and p-ERK1/2 (2.4-fold ± 0.5; $P < .05$), whereas IL-6 only induced p-ERK1/2 (2.4-fold ± 0.2; $P < .05$) (Figure 4*B*). Hence, the antrum and fundus respond differently to gp130 stimulation. Antrum responds only to IL-11 via STAT3, whereas fundus responds to both IL-11 and IL-6 predominantly via ERK1/2, but IL-11 also induces STAT3.

IL-11 Regulates Proliferative and Apoptotic Genes in the Stomach Important in Gastric Pathology

To identify gastric IL-11–regulated genes we performed cDNA microarray on antral tissue from IL-11–treated WT mice (5 μg IP) compared with sham. The 100 most differentially expressed genes were chosen for evaluation (supplementary Table 3; see supplementary material online at www.gastrojournal.org). A proportion, including SOCS-3, STAT3, and gp130, are known IL-11 targets.

To identify IL-11–responsive genes important for epithelial homeostasis, proliferative and apoptotic genes were selected from the microarray, changes confirmed by quantitative PCR, and expression was compared with gp130$^{757F/F}$ antral tumors and hyperplastic HKβ-/- fundus. Gene expression in HKβ-/- also was compared with HKβ-/-IL-11Rα-/-. Four genes were increased significantly: RegIIIβ, RegIIIγ, gremlin-1, and clusterin; and one gene, growth arrest specific-1 (GAS-1), was decreased in IL-11–treated antrum and gp130$^{757F/F}$ antral tumors (Figure 5). Apart from gremlin-1, this pattern was maintained in HKβ-/- hyperplastic fundus (Figure 5). Furthermore, RegIIIβ, RegIIIγ, and gremlin-1 were decreased significantly in HKβ-/-IL-11Rα-/- fundus compared with HKβ-/-, correlating with absence of IL-11 and reduced hyperplasia (Figure 5).

To determine the importance of this gene signature in human gastric cancer development, we tested expression in surgical specimens from CagA-positive *H pylori*–infected and gastric cancer patients both within the cancer and in adjacent nonneoplastic mucosa (supplementary Table 2; see supplementary material online at www.gastrojournal.org). Expression was compared with disease-free individuals. RegIIIα (human homologue of mouse RegIIIβ) and RegIIIγ were up-regulated in *H pylori* infection (Figure 5*A* and *B*), all 5 genes were up-regulated in nonneoplastic mucosa adjacent to cancer (Figure 5), and up-regulation of gremlin-1 and GAS-1 was maintained in cancer (Figure 5*D* and *E*). This shows that although the Reg genes seem important in the very early stages of the disease and gremlin-1 and GAS-1 seem important in the late stages, expression of the whole gene signature is evident in nonneoplastic tissue adjacent to cancer, which by definition is at high risk for cancer development, suggesting these genes play a role in gastric cancer progression.

Chronic IL-11 Treatment Decreases Apoptosis in the Antrum Via Increased p-AKT

To determine if chronic IL-11 sustained the gene signature and caused preneoplastic changes in normal stomach, WT mice were administered IL-11 (5 μg IP) every 6 hours (to maintain elevated antral-p-STAT3, data not shown) for 7 days (WTcIL-11). Apart from GAS-1 in antrum, the IL-11 gene signature was altered consistently in antrum and fundus of WTcIL-11 mice (supplementary Figure 1; see supplementary material online at www.gastrojournal.org).

In WTcIL-11 antrum, p-STAT3 was increased 2.4-fold (±0.5; n = 6; $P < .05$) and ERK1/2 was not activated (Figure 6*A*), in the same deregulated pattern seen in gp130$^{757F/F}$ antral tumors. In the fundus, STAT3 was not activated and p-ERK1/2 was increased 2.3-fold (±0.3;

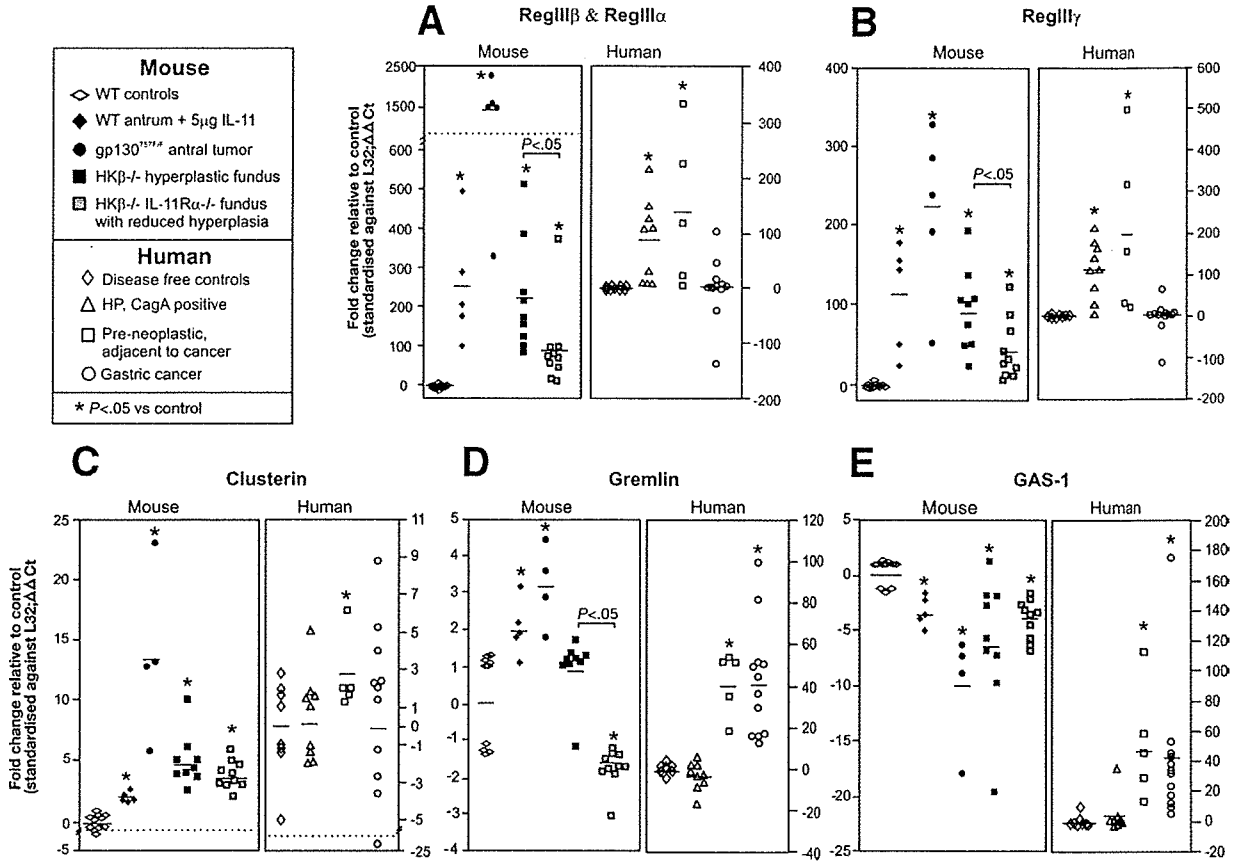

Figure 5. (*A*) RegIIIβ (hRegIIIα), (*B*) RegIIIγ, (*C*) clusterin, (*D*) gremlin, and (*E*) GAS-1 were measured by quantitative PCR, standardized to housekeeper L32, and expressed as fold change vs controls (ΔΔCt). Controls were WT littermates (mouse) or disease-free samples (human beings). *$P < .05$ compared with control. *Bars* indicate mean.

n = 6; $P < .05$) (Figure 6*A*), emphasizing that antrum and fundus respond differently to gp130 stimulation.

Apart from STAT and ERK activation, gp130 binding also leads to phosphorylation of phosphoinositide 3-kinase and activation of the serine/threonine protein kinase Akt pathway.[24] p-AKT levels were increased 2.1-fold (±0.1; n = 6; $P < .05$) in antrum and were unchanged in fundus of WTcIL-11 mice (Figure 6*A*). Because p-AKT is potently anti-apoptotic,[25] we quantified gastric epithelial apoptosis in WTcIL-11 mice by performing terminal deoxynucleotidyl transferase–mediated deoxyuridine triphosphate nick-end labeling (data not shown) and cleaved caspase-3 immunohistochemistry (Figure 6*B*). Apoptosis was reduced by 80% in WTcIL-11 antrum and unchanged in fundus (Figure 6*C*), showing that IL-11 can decrease apoptosis in the antrum, most likely through modulation of p-AKT.

Chronic IL-11 Treatment Induces Pretumorigenic Changes in Antrum and Fundus

To determine if chronic IL-11 affected proliferation, Ki-67 immunohistochemistry was performed (Figure 7*A* and *D*). In antrum, chronic IL-11 administration leads to significantly reduced epithelial cell proliferation (Figure 7*Ai* and ii and *B*). To determine if this was indicative of preneoplastic changes, proliferation was examined in 6-week-old WT and gp130$^{757F/F}$ mice (Figure 7*Aiii* and iv). Antral mucosa of 6-week-old gp130$^{757F/F}$ mice had tumors and adjacent, histologically unaffected, but pretumorigenic mucosa (Figure 7iv–vi). Pretumorigenic gp130$^{757F/F}$ antrum also had reduced epithelial cell proliferation compared with age-matched controls, whereas adjacent tumors had significantly increased proliferation (Figure 7*Aiii*–vi and *C*). Unlike the tumors, epithelial cell proliferation is decreased in pretumorigenic gp130$^{757F/F}$ tissue and this pattern can be similarly induced by IL-11 treatment for 1 week.

Conversely, in the fundus of WTcIL-11 mice, epithelial cell proliferation was increased significantly (Figure 7*Di* and ii and *E*), a hallmark of disease in HKβ-/- hyperplastic fundus. Furthermore, epithelial cell proliferation was decreased significantly in HKβ-/-IL-11Rα-/- compared with HKβ-/- fundus (Figure 7*Diii* and iv and *F*), thereby providing a mechanism for reduced hyperplasia here and showing that IL-11 can drive proliferation in the fundus.

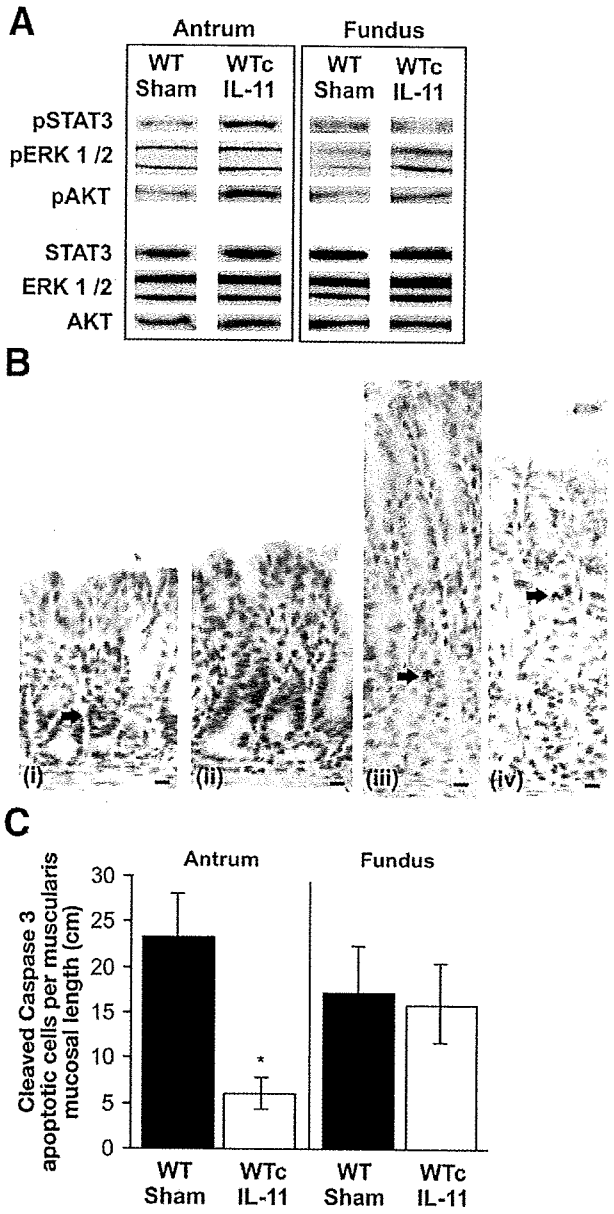

Figure 6. STAT3, p-STAT3, ERK 1/2, p-ERK 1/2, AKT, and p-AKT were measured by immunoblotting stomach from WT mice administered 5 μg IL-11 (WTcIL-11) or saline (sham) every 6 hours for 7 days. (*A*) Quantitation densitometry was performed and phosphorylated total protein was calculated from duplicate blots; representative bands are shown. Immunohistochemical localized cleaved caspase-3 apoptotic cells (*arrows*) in (*B*) sham antrum (i) and fundus (iii) and (*C*) WTcIL-11 antrum (ii) and fundus (iv) were counted by light microscopy and standardized against muscularis mucosal length (cm). *Scale bar*, 10 μm. $^{*}P < .05$ compared with control ($n \geq 7$).

Together, this directly shows that IL-11 can modulate antral and fundic epithelial proliferation, correlating with pathology in both mucosae.

Discussion

High IL-11 expression correlated with gastric pathology not only in gp130$^{757F/F}$ mice, with pathology driven by a mutation on gp130, but also in 3 other gastric models that are independent of gp130, suggesting that IL-11 contributes to pathogenesis of the stomach in a diverse array of settings. Furthermore, we show that IL-11 is important in human gastric cancer, where expression was increased significantly, as well as in gastric cancer progression because IL-11 was increased in mucosa adjacent to a cancer, which by definition has a high risk for cancer development. This implies that IL-11 may play crucial roles in gastric cancer development.

In gp130$^{757F/F}$ mice, the gp130 (Y757F) mutation abolishes SHP2 and SOCS3 binding, ablating Ras/ERK/AP-1 activation and leading to subsequent imbalanced signaling output, skewed toward hyperactivated STAT3.[13] Hyperactivated STAT3 causes antral tumors in these mice.[15] In WT antrum, a single dose of IL-11 caused exactly the same pattern of hyperactivated STAT3, with no induction of p-ERK. Moreover, we and Ernst et al[22] showed that loss of IL-11Rα ablates hyperactivated STAT3 and consequent tumors in gp130$^{757F/F}$ mice. IL-6 did not induce the same signaling pattern in the antrum, commensurate with the pathology of gp130$^{757F/F}$ IL-6-/- mice, in which deletion of IL-6 did not affect p-STAT3 or tumorigenesis, despite IL-6 being increased consistently in tumors similar to IL-11.[26] In the normal antrum IL-11 causes imbalanced gp130 signaling, skewing it toward hyperactivated STAT3, which causes tumors in gp130$^{757F/F}$ mice. Because activated STAT3 also correlates with reduced survival in gastric cancer patients,[11] IL-11 may be an independent risk factor for disease development.

We explored the idea that IL-11 can independently contribute to gastric pathology by examining stomachs from HKβ-/-IL-11Rα-/- mice. HKβ-/- mice have high fundic IL-11 expression and hyperplasia driven by hypergastrinemia.[23,27] Significantly, HKβ-/- IL-11Rα-/- mice had reduced fundic hyperplasia and proliferation, despite ongoing hypergastrinemia similar to HKβ-/- mice. Furthermore, expression of RegIIIβ, RegIIIγ, and gremlin all were reduced significantly in HKβ-/-IL-11Rα-/- mice compared with HKβ-/- mice. This shows that IL-11 can affect gastric pathology in mouse models independent of gp130 mutation and that reduced IL-11 signaling and expression of target genes can independently limit pathology, even in a hypergastrinemic environment.

gp130$^{757F/F}$ tumors initiate in the antrum, progressing to the fundus over time, and altered signaling via STAT3 and ERK1/2 is implicated in this pathology.[14] We compared gp130 signaling between the antrum and fundus and showed that gp130 stimulation induces a different signaling profile in each mucosa. Although the antral response was skewed to oncogenic p-STAT3, the fundus had a more balanced gp130 output with both IL-6 and IL-11 inducing p-ERK. This may provide some insight as to why gp130$^{757F/F}$ tumors initiate in the antrum and not the fundus, and suggests that each mucosa may have a varied physiologic response to excessive gp130 signaling.

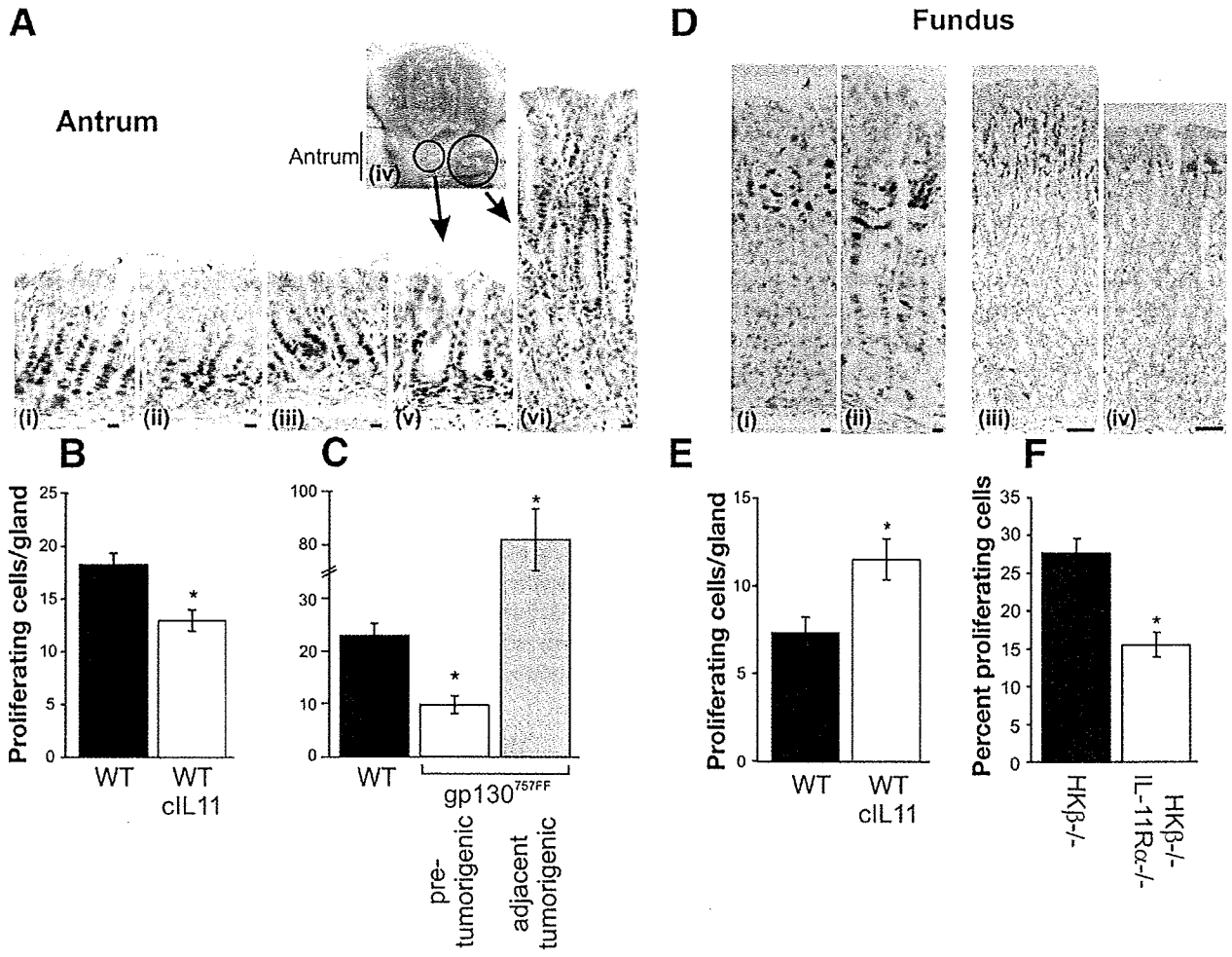

Figure 7. (*A*) Ki-67 immunohistochemically localized proliferating cells in antrum of WT sham (i), WTclL-11 (ii), 6-week-old WT (iii), and $gp130^{757F/F}$ separated into pretumorigenic (iv, *small circle*; and v) or tumorigenic (iv, *large circle*; and vi). (*B* and *C*) Ki-67–positive cells were point counted per gland from digital images. Similar analysis was performed in fundus: WT sham (*Di* and *E*), WTclL-11 (*Dii* and *E*), HKβ-/- (*Diii*), and HKβ-/-IL-11Rα-/- (*Div*), except (*F*) proliferating cells were expressed as a percentage of total cells in HKβ-/- because glands were difficult to discern. *Scale bar*, 10 μm. $^*P < .05$ compared with control ($n \geq 7$).

To determine the transcriptional outcome of IL-11/STAT3 overexpression, we identified a gastric IL-11 responsive gene signature of 5 genes. This signature, RegIII-β (RegIIIα in human beings), RegIII-γ, bone morphogenic protein (BMP)-antagonist gremlin-1, cytoprotective clusterin, and GAS-1, changed similarly in WT antrum after IL-11 administration and in $gp130^{757F/F}$ and HKβ-/- mouse models.

The genes in this signature are reported to be differentially involved in proliferation, apoptosis, and differentiation with their effect on these outcomes variable depending on the stimulus and site of expression. Reg family proteins have a complex nomenclature and overlapping functions.[28] Expression of RegIα correlates with poor clinical outcome in gastric cancer, is increased in hypergastrinemia and *H pylori* infection, and is proliferative in vitro.[29,30] STAT3 and Reg1α reduce apoptosis through p-AKT induction, and RegIII-β is anti-apoptotic.[31] gremlin-1 binds and blocks BMP2, BMP4, and BMP7,[32] and BMP2 is pro-apoptotic, suggesting that gremlin-1 blocks apoptosis.[33] gremlin-1 also is proliferative for colonic stem cells and some cancers.[34] Clusterin is implicated in numerous pathophysiologic processes,[35] is increased in antropyloric tumors of trefoil factor-1-/- mice,[36] correlates with progression of various cancers, and phase I clinical trials are in place to test its inhibitors clinically.[37,38] GAS-1, originally shown to induce growth arrest,[39] also antagonizes sonic hedgehog.[40] Although the function of GAS-1 in the stomach is largely unknown, reduced sonic hedgehog signaling correlates with gastric cancer progression.[41]

To investigate the importance of the IL-11 gene signature in human disease, we examined expression in tissues from patients with gastric pathology corresponding to several stages of the Correa[1] model of gastric cancer. That is, disease-free, CagA-positive, *H pylori* and gastric cancer patients, either in nonneoplastic tissue adjacent to a tumor but with

intestinal-metaplasia or chronic gastritis or tumor tissue. Although RegIIIα and RegIIIβ were increased in *H. pylori* infection, and gremlin and GAS-1 were increased in cancer, all 5 genes were increased in nonneoplastic mucosa sampled adjacent to gastric cancer, which also had high IL-11 expression. That GAS-1 expression was decreased in mouse and increased in human beings with increased IL-11 levels suggests it is differentially regulated, although because it was significantly different in both supports the many reported functions of GAS-1. These data show that IL-11 and its gene signature all were up-regulated in nonneoplastic tissue adjacent to cancer, which has a high risk for cancer spread, suggesting that IL-11 may be a key independent regulator of events predisposing to adenocarcinoma development.

To investigate if increased IL-11 alone was sufficient to induce a tumor, we treated WT mice chronically with IL-11 (WTcIL-11) for 1 week. Treatment for only 1 week did not result in tumor development, despite expression of the IL-11 gene signature. However, we found that gastric epithelial cell dynamics were altered significantly by this treatment. In the fundus, epithelial cell proliferation was increased. This is in keeping with reduced proliferation in HKβ-/-IL-11Rα-/- mice and directly shows that IL-11 can drive fundic epithelial cell proliferation, an established step in the progression toward pathology.

Conversely, in WTcIL-11 antrum, epithelial cell apoptosis and proliferation were decreased. This seems to contradict the IL-11–dependent increased proliferation seen in the antrum of gp130$^{757F/F}$ mice. However, younger gp130$^{757F/F}$ mice with histologically normal but preneoplastic antral mucosa also display reduced proliferation. We believe that hyperstimulation of the IL-11/gp130 signaling pathway in the antrum initially affects the mucosa by decreasing proliferation and decreasing apoptosis. These static conditions allow for an accumulation of cells with a greater half-life and increased potential to develop precancerous changes.

That proliferation and apoptosis in antrum and fundus were differentially affected by chronic IL-11 treatment, even when the same gene signature was observed, suggests that its mechanism of action depends on the anatomic target site. These differences are supported by the varied gp130 signaling outputs induced in each mucosa, the variable effects of the site, and timing of signature gene expression, as well as the vastly different turnover times and differentiation profiles of antral and fundic epithelial cells.[42] Precedence for this variation comes from studies of *H pylori*–infected patients, where proliferation and apoptosis are differentially affected according to stomach site[43] and conflicting data on the effect of *H pylori* on cell cycle, which also may reflect variance in cellular origin.[44–46] Moreover, all of the genes in the IL-11 signature have multiple effects on proliferation and apoptosis depending on cell type.[29,31,33,34,39,40,47] The unifying outcome is that chronic IL-11 always results in disrupted homeostatic epithelial cell turnover, an initiating step toward pathology. This suggests that IL-11 and its target genes are important in the development of gastric disease regardless of location, further shown by the consistent increase of IL-11 and its associated gene signature in tumor or hyperplasia from either antral or fundic origin in both mouse and human beings.

We have shown that IL-11 expression is increased in 4 diverse mouse models of gastric tumorigenesis or hyperplasia, as well as in preneoplastic and cancerous tissue from human stomach adenocarcinomas. In addition, we have characterized a novel IL-11–induced gene signature evident in pathogenic mouse models and, most importantly, in preneoplastic gastric tissue. Just 1 week of exposure to IL-11 induces this same gene signature commensurate with alterations in the carefully balanced epithelial cell commitment and proliferation program of the stomach, a known step in the progression toward cancer. Furthermore, IL-11 signaling in the antral stomach, where most adenocarcinomas originate, is biased strongly to phosphorylated STAT3, an oncogenic transcription factor when chronically activated. Together, these data support a novel regulatory role for IL-11, particularly in early gastric adenocarcinoma development, and highlights the need for the development of therapeutic inhibitors of IL-11 or its signaling pathways.

Supplementary Data

Note: To access the supplementary material accompanying this article visit the online version of *Gastroenterology* at www.gastrojournal.org, and at doi: 10.1053/j.gastro.2008.12.003.

References

1. Correa P. The biological model of gastric carcinogenesis. IARC Sci Publ 2004:301–310.
2. Heinrich PC, Behrmann I, Haan S, et al. Principles of interleukin (IL)-6-type cytokine signalling and its regulation. Biochem J 2003; 374:1–20.
3. Jackson CB, Judd LM, Menheniott TR, et al. Augmented gp130-mediated cytokine signalling accompanies human gastric cancer progression. J Pathol 2007;213:140–151.
4. Nakayama T, Yoshizaki A, Izumida S, et al. Expression of interleukin-11 (IL-11) and IL-11 receptor alpha in human gastric carcinoma and IL-11 upregulates the invasive activity of human gastric carcinoma cells. Int J Oncol 2007;30:825–833.
5. Yoshizaki A, Nakayama T, Yamazumi K, et al. Expression of interleukin (IL)-11 and IL-11 receptor in human colorectal adenocarcinoma: IL-11 up-regulation of the invasive and proliferative activity of human colorectal carcinoma cells. Int J Oncol 2006; 29:869–876.
6. Orazi A, Du X, Yang Z, et al. Interleukin-11 prevents apoptosis and accelerates recovery of small intestinal mucosa in mice treated with combined chemotherapy and radiation. Lab Invest 1996;75: 33–42.
7. Potten CS. Protection of the small intestinal clonogenic stem cells from radiation-induced damage by pretreatment with interleukin 11 also increases murine survival time. Stem Cells 1996; 14:452–459.
8. Qiu BS, Pfeiffer CJ, Keith JC Jr. Protection by recombinant human interleukin-11 against experimental TNB-induced colitis in rats. Dig Dis Sci 1996;41:1625–1630.

9. Wen CY, Ito M, Matsuu M, et al. Mechanism of the antiulcerogenic effect of IL-11 on acetic acid-induced gastric ulcer in rats. Life Sci 2002;70:2997–3005.
10. Wen CY, Ito M, Wang H, et al. IL-11 up-regulates Tie-2 expression during the healing of gastric ulcers in rats. World J Gastroenterol 2003;9:788–790.
11. Yakata Y, Nakayama T, Yoshizaki A, et al. Expression of p-STAT3 in human gastric carcinoma: significant correlation in tumour invasion and prognosis. Int J Oncol 2007;30:437–442.
12. Higashi H, Tsutsumi R, Muto S, et al. SHP-2 tyrosine phosphatase as an intracellular target of *Helicobacter pylori* CagA protein. Science 2002;295:683–686.
13. Tebbutt NC, Giraud AS, Inglese M, et al. Reciprocal regulation of gastrointestinal homeostasis by SHP2 and STAT-mediated trefoil gene activation in gp130 mutant mice. Nat Med 2002;8:1089–1097.
14. Judd LM, Alderman BM, Howlett M, et al. Gastric cancer development in mice lacking the SHP2 binding site on the IL-6 family co-receptor gp130. Gastroenterology 2004;126:196–207.
15. Judd LM, Bredin K, Kalantzis A, et al. STAT3 activation regulates growth, inflammation, and vascularization in a mouse model of gastric tumorigenesis. Gastroenterology 2006;131:1073–1085.
16. Scarff KL, Judd LM, Toh BH, et al. Gastric H(+),K(+)-adenosine triphosphatase beta subunit is required for normal function, development, and membrane structure of mouse parietal cells. Gastroenterology 1999;117:605–618.
17. Oshima H, Oshima M, Inaba K, et al. Hyperplastic gastric tumors induced by activated macrophages in COX-2/mPGES-1 transgenic mice. EMBO J 2004;23:1669–1678.
18. Oshima H, Matsunaga A, Fujimura T, et al. Carcinogenesis in mouse stomach by simultaneous activation of the Wnt signaling and prostaglandin E2 pathway. Gastroenterology 2006;131:1086–1095.
19. Nandurkar HH, Robb L, Tarlinton D, et al. Adult mice with targeted mutation of the interleukin-11 receptor (IL11Ra) display normal hematopoiesis. Blood 1997;90:2148–2159.
20. Boussioutas A, Li H, Liu J, et al. Distinctive patterns of gene expression in premalignant gastric mucosa and gastric cancer. Cancer Res 2003;63:2569–2577.
21. Smyth GK, Speed T. Normalization of cDNA microarray data. Methods 2003;31:265–273.
22. Ernst M, Najdovska M, Grail D, et al. STAT3 and STAT1 mediate IL-11-dependent and inflammation-associated gastric tumorigenesis in gp130 receptor mutant mice. J Clin Invest 2008;118:1727–1738.
23. Franic TV, Judd LM, Robinson D, et al. Regulation of gastric epithelial cell development revealed in H(+)/K(+)-ATPase beta-subunit- and gastrin-deficient mice. Am J Physiol Gastrointest Liver Physiol 2001;281:G1502–G1511.
24. Kamimura D, Ishihara K, Hirano T. IL-6 signal transduction and its physiological roles: the signal orchestration model. Rev Physiol Biochem Pharmacol 2003;149:1–38.
25. Franke TF, Kaplan DR, Cantley LC. PI3K: downstream AKTion blocks apoptosis. Cell 1997;88:435–437.
26. Howlett M, Judd LM, Jenkins B, et al. Differential regulation of gastric tumor growth by cytokines that signal exclusively through the coreceptor gp130. Gastroenterology 2005;129:1005–1018.
27. Franic TV, van Driel IR, Gleeson PA, et al. Reciprocal changes in trefoil 1 and 2 expression in stomachs of mice with gastric unit hypertrophy and inflammation. J Pathol 2005;207:43–52.
28. Graf R, Schiesser M, Reding T, et al. Exocrine meets endocrine: pancreatic stone protein and regenerating protein—two sides of the same coin. J Surg Res 2006;133:113–120.
29. Kadowaki Y, Ishihara S, Miyaoka Y, et al. Reg protein is overexpressed in gastric cancer cells, where it activates a signal transduction pathway that converges on ERK1/2 to stimulate growth. FEBS Lett 2002;530:59–64.
30. Fukui H, Kinoshita Y, Maekawa T, et al. Regenerating gene protein may mediate gastric mucosal proliferation induced by hypergastrinemia in rats. Gastroenterology 1998;115:1483–1493.
31. Sekikawa A, Fukui H, Fujii S, et al. REG I{alpha} protein mediates an anti-apoptotic effect of STAT3 signaling in gastric cancer cells. Carcinogenesis 2008;29:76–83.
32. Hsu DR, Economides AN, Wang X, et al. The Xenopus dorsalizing factor Gremlin identifies a novel family of secreted proteins that antagonize BMP activities. Mol Cell 1998;1:673–683.
33. Merino R, Rodriguez-Leon J, Macias D, et al. The BMP antagonist Gremlin regulates outgrowth, chondrogenesis and programmed cell death in the developing limb. Development 1999;126:5515–5522.
34. Kosinski C, Li VS, Chan AS, et al. Gene expression patterns of human colon tops and basal crypts and BMP antagonists as intestinal stem cell niche factors. Proc Natl Acad Sci U S A 2007;104:15418–15423.
35. Rosenberg ME, Silkensen J. Clusterin: physiologic and pathophysiologic considerations. Int J Biochem Cell Biol 1995;27:633–645.
36. Torres LF, Karam SM, Wendling C, et al. Trefoil factor 1 (TFF1/pS2) deficiency activates the unfolded protein response. Mol Med 2002;8:273–282.
37. Miyake H, Hara I, Fujisawa M, et al. The potential of clusterin inhibiting antisense oligodeoxynucleotide therapy for prostate cancer. Expert Opin Investig Drugs 2006;15:507–517.
38. Gleave M, Chi KN. Knock-down of the cytoprotective gene, clusterin, to enhance hormone and chemosensitivity in prostate and other cancers. Ann N Y Acad Sci 2005;1058:1–15.
39. Del Sal G, Collavin L, Ruaro ME, et al. Structure, function, and chromosome mapping of the growth-suppressing human homologue of the murine gas1 gene. Proc Natl Acad Sci U S A 1994;91:1848–1852.
40. Lee CS, Buttitta L, Fan CM. Evidence that the WNT-inducible growth arrest-specific gene 1 encodes an antagonist of sonic hedgehog signaling in the somite. Proc Natl Acad Sci U S A 2001;98:11347–11352.
41. van den Brink GR. Hedgehog signaling in development and homeostasis of the gastrointestinal tract. Physiol Rev 2007;87:1343–1375.
42. Karam SM. Lineage commitment and maturation of epithelial cells in the gut. Front Biosci 1999;4:D286–D298.
43. Kitsanta P, Triantafyllou K, Chatziargyriou M, et al. Gastric mucosa epithelial cell kinetics are differentiated by anatomic site and *Helicobacter pylori* infection. Dig Dis Sci 2005;50:1087–1091.
44. Ahmed A, Smoot D, Littleton G, et al. *Helicobacter pylori* inhibits gastric cell cycle progression. Microbes Infect 2000;2:1159–1169.
45. Fan XG, Kelleher D, Fan XJ, et al. *Helicobacter pylori* increases proliferation of gastric epithelial cells. Gut 1996;38:19–22.
46. Moss SF, Calam J, Agarwal B, et al. Induction of gastric epithelial apoptosis by *Helicobacter pylori*. Gut 1996;38:498–501.
47. Pucci S, Bonanno E, Pichiorri F, et al. Modulation of different clusterin isoforms in human colon tumorigenesis. Oncogene 2004;23:2298–2304.

Received March 28, 2008. Accepted December 1, 2008.

Reprint requests

Address requests for reprints to: Louise M. Judd, PhD, Royal Children's Hospital, Flemington Road, Parkville, Melbourne, Victoria, Australia. e-mail: lmj@unimelb.edu.au; fax: (613) 9936-6501.

Conflicts of interest

The authors disclose no conflicts.

Supplementary Table 1. Primer Sequences for IL-11Rα Genotyping and Real-Time PCR (Sybr) Analysis

Gene	Forward primer	Reverse primer	Temperature, °C	Cycles
IL-11Rα Genotyping	F1.GGCTCCCGTCATTACCTACA F2.ACTTGTGTAGCGCCAAGTGC	R1.AGCAGTCCTACCCGCTACAA	60	35
mGastrin Sybr	CACTTCATAGCAGACCTGTCCAA	CATCCGTAGGCCTCTTCTTCTTC	—	—
mRegIIIβ Sybr	GAACCCATCTACTGCCTTAGACC	CTTCACATTTTGTCCCTTGTC	—	—
mRegIIIγ Sybr	ACGAATCCTTCCTCTTCCTCAG	GTCTTCACATTTGGGATCTTGC	—	—
mClusterin Sybr	GAAGGGCCAGTGTGAAAAGTG	TTAGCCTGGGCAGGATTGTT	—	—
mGremlin-1 Sybr	TGAAGCAGTGCCGTTGCATA	TGAATGTGCCCGCTTTGA	—	—
mGAS-1 Sybr	GCCGCTACCTGGCCTACTG	GGCACGGCCAGCATGT	—	—
hRegIIIα Sybr	TCTGGATTGGGCTCCATGAC	CTCCCAACCTTCTCCATTGG	—	—
hRegIIIγ Sybr	TCTGGATTGGGCTCCATGAC	GCTACTCCACTCCCATCCATCT	—	—
hClusterin Sybr	CCGCCAGCTTGAGGAGTTC	GAGTCGATGCGGTCACCAT	—	—
hGremlin-1 Sybr	CTCAGCGCCACGCGTCGAA	TCCCTTCAGCAGCCGGCAG	—	—
hGAS-1 Sybr	CGCGCATGGATTTATGAAGA	CGGAGCCGGTGGAAAAGT	—	—

Supplementary Table 2. Gastric Specimen Diagnosis and Demographic Data

Age, *y*	Sex	Country	HUT	CagA	Gastritis, Y/N	IM, Y/N	Dysplasia, Y/N	Site of tumor	Type	T stage	N stage	M stage	AJCC	Sample, C/A
Disease free														
45	M	Australia	Neg	Neg	N	N	N	—	—	—	—	—	—	—
46	M	Australia	Neg	Neg	N	N	N	—	—	—	—	—	—	—
67	M	Australia	Neg	Neg	N	N	N	—	—	—	—	—	—	—
58	M	Australia	Neg	Neg	N	N	N	—	—	—	—	—	—	—
34	F	Australia	Neg	Neg	N	N	N	—	—	—	—	—	—	—
39	M	Australia	Neg	Neg	N	N	N	—	—	—	—	—	—	—
56	M	Australia	Neg	Neg	N	N	N	—	—	—	—	—	—	—
68	F	Australia	Neg	Neg	N	N	N	—	—	—	—	—	—	—
H pylori, CagA-positive														
34	M	Australia	Pos	Pos	Y	N	N	—	—	—	—	—	—	—
58	M	Australia	Pos	Pos	Y	N	N	—	—	—	—	—	—	—
68	M	Australia	Pos	Pos	Y	N	N	—	—	—	—	—	—	—
39	F	Australia	Pos	Pos	N	N	N	—	—	—	—	—	—	—
49	F	Australia	Pos	Pos	Y	N	N	—	—	—	—	—	—	—
34	F	Australia	Pos	Pos	Y	N	N	—	—	—	—	—	—	—
36	F	Australia	Pos	Pos	Y	N	N	—	—	—	—	—	—	—
47	M	Australia	Pos	Pos	Y	N	N	—	—	—	—	—	—	—
53	M	Australia	Pos	Pos	Y	N	N	—	—	—	—	—	—	—
Gastric cancer patients														
73	M	Australia	—	—	Y	Y	N	Antrum	—	3	1	0	3A	A
70	M	Australia	—	—	Y	N	N	GES	—	3	1	0	3A	A
55	M	Australia	—	—	Y	Y	N	Body	—	3	1	0	3A	A
78	M	Australia	—	—	Y	N	N	Body	—	3	0	0	2	A
80	F	Australia	—	—	Y	Y	N	Antrum	—	3	1	0	3A	A
44	M	Australia	—	—	Y	—	Y	Antrum	Diffuse	3	1	0	3A	C
78	M	Australia	—	—	Y	—	Y	Body	Intestinal	3	0	0	2	C
53	M	Australia	—	—	Y	—	Y	Body	Intestinal	2	0	0	1B	C
67	M	Australia	—	—	Y	—	Y	Body	Mixed	3	2	0	3B	C
69	M	Australia	—	—	Y	—	Y	Body	Intestinal	3	0	0	2	C
75	F	Australia	—	—	Y	—	Y	Body	Diffuse	1	1	0	1B	C
61	F	Australia	—	—	Y	—	Y	GES	Intestinal	2	1	0	2	C
55	M	Australia	—	—	Y	—	Y	Body	Intestinal	3	2	0	3B	C
33	F	Australia	—	—	Y	—	Y	Body	Diffuse	3	1	0	3A	C

NOTE. Demographic data are from disease-free, *H pylori*, CagA-positive, and gastric cancer patients. Staging of gastric cancer specimens was performed according to the TNM staging system, maintained by the American Joint Committee on Cancer.
A, adjacent to the cancer; C, within the cancer; GES, gastroesophageal junction; Neg, negative; Pos, positive; —, not applicable for that specimen.

Supplementary Table 3. Genes Regulated by IL-11 in the Gastric Antral Mucosa

ID (Acc)	Name	Symbol	Fold change	*P* value	Expression in response to IL-11
NM_011036	Pancreatitis-associated protein	Pap	6.43	.1422	Up √
NM_011260	Regenerating islet-derived 3 γ	Reg3g	3.18	.1152	Up √
NM_033075	DNA segment, Chr 17, human D6S56E 5	D17H6S56E-5	3.00	.0679	Up
NM_020574	Potassium voltage-gated channel, Isk-related subfamily, gene 3	Kcne3	2.95	.1004	Up
NM_008397	Integrin α 6	Itga6	2.53	.1592	Up x
NM_010276	GTP binding protein (gene overexpressed in skeletal muscle)	Gem	2.50	.1422	Up
AK020461	Mortality factor 4–like 1	Morf4l1	2.21	.0679	Up
BC006651	STEAP family member 4	Steap4	2.17	.1207	Up √
NM_011580	Thrombospondin 1	Thbs1	2.00	.1864	Up √
AF294329	Polymerase (DNA-directed), δ 3, accessory subunit	Pold3	1.95	.1004	Up
NM_026010	RIKEN cDNA 2610209A20 gene	2610209A20Rik	1.92	.1107	Up
NM_007679	CCAAT/enhancer binding protein (C/EBP), δ	Cebpd	1.89	.1592	Up
NM_009621	A disintegrin-like and metallopeptides (reprolysin type) with thrombospondin type 1 motif, 1	Adamts1	1.89	.1422	Up √
AF403429	Leucine-rich α-2-glycoprotein 1	Lrg1	1.86	.2063	Up
AK019034	Cysteine-rich secretory protein LCCL domain containing 2	Crispld2	1.81	.1592	Up
NM_008428	Potassium inwardly rectifying channel, subfamily J, member 8	Kcnj8	1.80	.2134	Up
BC005613	Mortality factor 4–like 1	Morf4l1	1.78	.1526	Up
BC004847	Serine carboxypeptidase 1	Scpep1	1.76	.0679	Up
NM_016748	Cytidine 5′-triphosphate synthase	Ctps	1.75	.1789	Up
NM_008329	Interferon-activated gene 203	Ifi203	1.74	.1422	Up
AK014511	RAS-like, family 12	Rasl12	1.72	.1570	Up
AK011895	Ectonucleoside triphosphate diphosphohydrolase 1	Entpd1	1.69	.1850	Up
AF395884	Calcium/calmodulin-dependent protein kinase II γ	Camk2g	1.68	.1776	Up
BC010821	Peptide YY	Pyy	1.67	.1702	Up
NM_013492	Clusterin	Clu	1.63	.2134	Up √
NM_008764	Tumor necrosis factor receptor superfamily, member 11b (osteoprotegerin)	Tnfrsf11b	1.62	.1768	Up
NM_011824	Gremlin 1	Grem1	1.60	.1422	Up √
U08378	Signal transducer and activator of transcription 3	Stat3	1.60	.1592	Up
NM_007711	Chloride channel 3	Clcn3	1.59	.1422	Up
NM_023284	Cell division cycle–associated 1	Cdca1	1.59	.1631	Up
NM_009838	Chaperonin subunit 6a (ζ)	Cct6a	1.56	.1864	Up
NM_008628	MutS homolog 2 (*Escherichia coli*)	Msh2	1.56	.2257	Up
NM_010128	Epithelial membrane protein 1	Emp1	1.53	.1592	Up x
AK013638	Solute carrier family 39 (zinc transporter), member 10	Slc39a10	1.52	.1930	Up
NM_008977	Protein tyrosine phosphatase, nonreceptor type 2	Ptpn2	1.51	.1768	Up
AJ236880	Tenascin C	Tnc	1.51	.2217	Up
NM_009890	Cholesterol 25-hydroxylase	Ch25h	1.51	.1284	Up
NM_024434	Leucine aminopeptidase 3	Lap3	1.49	.1842	Up
AK010399	Sorting nexin 10	Snx10	1.48	.0679	Up
AK017211	Interleukin 6 signal transducer	Il6st	1.47	.1592	Up
NM_008137	Guanine nucleotide binding protein, α 14	Gna14	1.45	.1197	Up
BC004827	Phosphoserine aminotransferase 1	Psat1	1.44	.2063	Up
AK008108	Sulfatase 2	Sulf2	1.44	.1207	Up
NM_031397	Bicaudal C homolog 1 (*Drosophila*)	Bicc1	1.43	.1592	Up
NM_008013	Fibrinogen-like protein 2	Fgl2	1.43	.1422	Up x
NM_008249	Transcription factor B2, mitochondrial	Tfb2m	1.43	.1592	Up
AK018314	Kelch-like 24 (*Drosophila*)	Klhl24	1.42	.1820	Up
NM_021525	RNA terminal phosphate cyclase-like 1	Rcl1	1.41	.1864	Up
NM_026041	RIKEN cDNA 2810430M08 gene	2810430M08Rik	1.41	.1864	Up
AK005460	Calponin 3, acidic	Cnn3	1.41	.2014	Up
NM_007707	Suppressor of cytokine signaling 3	Socs3	1.40	.1631	Up √
NM_009146	Ferric-chelate reductase 1	Frrs1	1.40	.1864	Up
AK018128	RIKEN cDNA 6330406I15 gene	6330406I15Rik	1.39	.2217	Up
BC008101	RAS-like, family 11, member B	Rasl11b	1.39	.1776	Up
NM_010330	Embigin	Emb	1.37	.1592	Up
NM_011593	Tissue inhibitor of metalloproteinase 1	Timp1	1.37	.1592	Up √
NM_008301	Heat shock protein 2	Hspa2	1.37	.1631	Up √
NM_030560	CDNA sequence BC003993	BC003993	1.37	.1864	Up

Table 3. Continued

ID (Acc)	Name	Symbol	Fold change	*P* value	Expression in response to IL-11
NM_019737	UDP-Gal:betaGlcNAc β 1,4-galactosyltransferase, polypeptide 6	B4galt6	1.36	.2239	Up
AK011330	SEH1-like (*Saccharomyces cerevisiae*)	Seh1l	1.35	.1631	Up
NM_013842	X-box binding protein 1	Xbp1	1.34	.2134	Up
NM_018745	Antizyme inhibitor 1	Azin1	1.34	.1592	Up
AK008774	Tyrosyl-tRNA synthetase 2 (mitochondrial)	Yars2	1.33	.1592	Up
U28068	Neurogenic differentiation 1	Neurod1	1.33	.1952	Up
BC005522	UTP20, small subunit (SSU) processome component, homolog (yeast)	Utp20	1.33	.2063	Up
BC006061	RIKEN cDNA 2010111I01 gene	2010111I01Rik	1.33	.2160	Up
NM_011609	Tumor necrosis factor receptor superfamily, member 1a	Tnfrsf1a	1.33	.2134	Up √
M33425	Janus kinase 1	Jak1	1.32	.1631	Up
NM_023799	Meningioma-expressed antigen 5 (hyaluronidase)	Mgea5	1.32	.1592	Up
U92454	WW domain binding protein 5	Wbp5	1.30	.2199	Up
NM_026330	Non-SMC element 1 homolog (*S cerevisiae*)	Nsmce1	1.29	.1702	Up
AJ304865	TNFAIP3 interacting protein 2	Tnip2	1.28	.1864	Up
AK013131	RIKEN cDNA 2810422B04 gene	2810422B04Rik	1.28	.1930	Up
NM_009373	Transglutaminase 2, C polypeptide	Tgm2	1.28	.2134	Up
AK013101	Integrator complex subunit 2	Ints2	1.27	.2063	Up
NM_009789	S100 calcium binding protein G	S100g	2.70	.1152	Down
NM_011740	Tyrosine 3-monooxygenase/tryptophan 5-monooxygenase activation protein, ζ polypeptide	Ywhaz	2.17	.1702	Down
NM_008086	Growth arrest specific 1	Gas1	2.10	.0346	Down √
AK008000	Alkaline phosphatase, intestinal	Alpi	1.80	.0679	Down
AK019848	Retinoic acid induced 17	Rai17	1.69	.1106	Down
AF031467	Branched chain aminotransferase 2, mitochondrial	Bcat2	1.63	.1768	Down
NM_019814	HIG1 domain family, member 1A	Higd1a	1.61	.1152	Down
NM_008095	Glioblastoma amplified sequence	Gbas	1.59	.1816	Down
AK004761	Ectonucleoside triphosphate diphosphohydrolase 4	Entpd4	1.55	.0679	Down
NM_010496	Inhibitor of DNA binding 2	Id2	1.53	.1930	Down
Y11505	Serine peptidase inhibitor, Kazal type 4	Spink4	1.52	.0679	Down
BC006054	RIKEN cDNA E130012A19 gene	E130012A19Rik	1.52	.2134	Down
NM_010356	Glutathione S-transferase, α 3	Gsta3	1.51	.1491	Down
AK004556	Solute carrier family 16 (monocarboxylic acid transporters), member 9	Slc16a9	1.49	.1592	Down
BC003491	Haloacid dehalogenase-like hydrolase domain containing 3	Hdhd3	1.46	.2134	Down
AK007745	RIKEN cDNA 1810041L15 gene	1810041L15Rik	1.45	.1422	Down
BC003457	Methionine adenosyltransferase II, β	Mat2b	1.44	.1592	Down
BC003429	ATPase, H+ transporting, lysosomal V1 subunit G1	Atp6v1g1	1.43	.1250	Down
BC004572	N-acylsphingosine amidohydrolase (acid ceramidase)-like	Asahl	1.41	.2257	Down
BC014708	Ependymin-related protein 2 (zebrafish)	Epdr2	1.41	.1503	Down
AK016217	RIKEN cDNA 4930564C03 gene	4930564C03Rik	1.38	.1728	Down
AF061972	HIV-1 tat interactive protein 2, homolog (human)	Htatip2	1.37	.1592	Down
AK003496	RIKEN cDNA 1110006G06 gene	1110006G06Rik	1.36	.1981	Down
NM_018784	ST3 β-galactoside α-2,3-sialyltransferase 6	St3gal6	1.32	.2063	Down
AJ249901	SPARC-related modular calcium binding 2	Smoc2	1.30	.2239	Down x

NOTE. Two-color cDNA microarray was performed on antral tissue from 5 WT mice treated with IL-11 (5 μg IP) compared with 5 saline-treated WT controls. The 100 most differentially expressed genes were selected. Many of these gene changes did not reach statistical significance because of replicate variability. Therefore, quantitative PCR was performed to validate a selection of 16 genes based on known biological activities. Twelve of 16 genes detected by microarray could be validated by quantitative PCR, producing 75% reliability of this microarray experiment.
√, genes that were tested and validated; x, genes that were tested and expression was unchanged.

Cancer Science
The official journal of the Japanese Cancer Association JCA

Bcl11b heterozygosity promotes clonal expansion and differentiation arrest of thymocytes in γ-irradiated mice

Rieka Go,[1] Satoshi Hirose,[1] Shinichi Morita,[1] Takashi Yamamoto,[1] Yoshinori Katsuragi,[1] Yukio Mishima[1,2] and Ryo Kominami[1,2,3]

[1]Department of Molecular Genetics, Graduate School of Medical and Dental Sciences; [2]Center for Transdisciplinary Research, Niigata University, Niigata, Japan

(Received November 19, 2009/Revised February 17, 2010/Accepted February 20, 2010/Accepted manuscript online February 27, 2010)

Bcl11b **encodes a zinc-finger transcription factor and functions as a haploinsufficient tumor suppressor gene. *Bcl11b*$^{KO/KO}$ mice exhibit differentiation arrest of thymocytes during β-selection as has been observed with other mouse models involving knockouts of genes in the Wnt/β-catenin signaling pathway. Recurrent chromosomal rearrangement at the *BCL11B* locus occurs in human T-cell leukemias, but it is not clear how such rearrangement would contribute to lymphomagenesis. To address this issue, we studied clonal cell growth, cell number, and differentiation of thymocytes in *Bcl11b*$^{KO/+}$ mice at different time points following γ-irradiation. Analysis of D-J rearrangement at the T cell receptor β-chain (*TCRβ*) locus and cell surface markers by flow cytometry revealed two distinct populations of clonally growing thymocytes. In one population, thymocytes share a common D-J rearrangement but retain the capacity to differentiate. In contrast, thymocytes in the second population have lost their ability to differentiate. Since the capacity to self renew and differentiate into multiple cell lineages are fundamental properties of adult stem cells, the differentiation competent population of thymocytes that we have isolated could potentially function as cancer stem cells. We also demonstrate increased expression of β-catenin, a well-known oncogenic protein, in *Bcl11b*$^{KO/+}$ thymocytes. Collectively, the *Bcl11b*$^{KO/+}$ genotype contributes to clonal expansion and differentiation arrest in part through an increase in the level of β-catenin. (*Cancer Sci* 2010)**

Cancer development is a complex, multistep process involving the acquisition of capabilities of cell autonomous proliferation and resistance to apoptosis.[1] This could be a consequence of a sequence of 4–6 mutations that are associated with different stages of the tumor progression.[2] Leukemia and lymphoma are malignancies of hematopoietic cells, and chronic myelogenous leukemia (CML) is among the malignancies characterized with frequently having the *bcr/abl* chimeric gene.[3] A two-step process is seen from CML to a subset of acute lymphoblastic leukemia (ALL) bearing *bcr/abl*, an aggressive blast crisis phase.[3–5] This transition requires an arrest of differentiation. Interestingly, CML already possesses intrinsic self-renewal capability like adult tissue stem cells and differentiate to mature, nontumorigenic blood cells.[6]

Bcl11b is a haploinsufficient tumor suppressor gene that was isolated from analyses of γ-ray induced mouse thymic lymphomas.[7–9] *Bcl11b*$^{KO/+}$ mice are susceptible to the development of thymic lymphomas,[9] suggesting that loss or decrease of Bcl11b function contributes to lymphomagenesis. Recurrent chromosomal rearrangement at the human *BCL11B* locus has been reported in T-cell leukemias,[10–12] but the effects of the rearrangement are not clear. *Bcl11b* encodes a zinc-finger transcription factor that is expressed in thymocytes, neurons and other tissues.[13–17] *Bcl11b*$^{KO/KO}$ and *Bcl11b*$^{lox/lox}$ mice show differentiation arrest of thymocytes during β-selection[13,14] and positive selection,[18] respectively; the arrest in the former seen at CD4 and CD8 double-negative (DN) and immature CD8 single-positive (ISP) cell stages before the CD4 and CD8 double-positive (DP) cell stage.[13,14] *Bcl11b*$^{KO/+}$ mice exhibit a substantial impairment of thymocyte differentiation in mouse embryos, although not as profound as that in *Bcl11b*$^{KO/KO}$ animals.[19] The arrest during β-selection is seen in many gene-knockout mice,[20] including genes affecting Wnt/β-catenin signaling.[21–23] As with oncogenesis, differentiation arrest may be a mechanism through which Bcl11b deficiency contributes to tumor development. However, *Bcl11b*$^{KO/KO}$ mice also show thymocyte apoptosis, and this anti-apoptotic property of Bcl11b seems to contradict a predicted proapoptotic function of tumor suppressors. The differentiation arrest and apoptosis are at least in part due to the decrease of pre-T cell receptor (TCR) signaling.[13,14]

Identical rearrangements of the *TCRβ* locus are seen in thymic lymphomas and this establishes clonality of the lymphomas.[24] Our previous studies demonstrated that such identical rearrangements were also found in γ-ray induced mouse atrophic thymuses, indicating the existence of clonally expanded thymocytes.[24,25] A significant percentage of those thymuses exhibited allelic loss of *Bcl11b*. These findings raise the question of how and at which stage does the *Bcl11b* heterozygous genotype contributes to lymphoma development. Here we studied the effect of *Bcl11b*$^{KO/+}$ genotype on β-catenin expression and on clonal cell proliferation of thymocytes in γ-irradiated mice. Our results provide an implication that the genotype contributes to clonal cell expansion and differentiation arrest, and the contribution may, in part, occur through an increase in β-catenin expression.

Materials and Methods

Mice and induction of atrophic thymus. *Bcl11b*$^{KO/+}$ mice with a BALB/c background were generated as described.[13] MSM mice were kindly supplied from Dr Shiroishi, National Institute of Genetics (NIG) (Mishima, Japan). *Bcl11b*$^{KO/+}$ mice were mated with MSM mice and their progeny were subjected to γ-irradiation of 3 Gy at 8 or 10 weeks of age. Left and right thymic lobes were separately isolated at 30, 60, or 80 days after the irradiation and subjected to analyses. Mice used in this study were maintained under specific pathogen-free conditions in the animal colony of Niigata University. All animal experiments complied with the guidelines for animal experimentation from the University animal ethics committee.

[3]To whom correspondence should be addressed.
E-mail: rykomina@med.niigata-u.ac.jp

doi: 10.1111/j.1349-7006.2010.01546.x

Flow cytometry. Flow cytometric analysis was performed as previously described.[13] In brief, single cell suspensions of thymocytes were prepared from thymus and 1–2 × 10^6 cells were incubated with antibodies in phosphate-buffered saline containing 2% fetal calf serum and 0.2% NaN_3 for 20 min at 4°C. The monoclonal antibodies (mAbs) used were: anti-CD4-PerCP-Cy5.5 or -APC (RM4-5), anti-CD8-PE (53-6.7), anti-TCRβ-FITC (H57-597; BioLegend, San Diego, CA, USA), anti-β-catenin-FITC (14; BD Biosciences, San Jose, CA, USA), and IL-7Rα-PE (SB/199, BioLegend, San Diego, CA, USA). They were purchased from eBioscience. To prevent nonspecific binding of mAbs, we added CD16/32 (93; eBioscience) before staining with labeled mAbs. Dead cells and debris were excluded from the analysis by appropriate gating of forward scatter (FSC) and side scatter (SSC). Cells were analyzed by a FACScan (Becton-Dickinson, Franklin Lakes, NJ, USA) flow cytometer, and data were analyzed using the Flow-Jo software (Tree-Star, Ashland, OR, USA).

For BrdU incorporation experiments, we injected mice intraperitoneally with 100 μL of BrdU solution (10 mg/mL) and thymus was isolated 1 h after. Thymocytes were prepared from the thymus and analyzed with the use of the BrdU Flow Kit (BD Pharmingen, San Diego, CA, USA) according to the manufacturer's instructions. In brief, cells were suspended at a concentration of 1–2 × 10^6 cells/mL, fixed, permeabilized, treated with DNase to expose incorporated BrdU, and incubated with a murine anti-BrdU antibody for 20 min at room temperature. After washing, cells were resuspended in 1 mL of PBS containing 20 μL of the 7AAD solution. Cells were resuspended in staining buffer and analyzed with the FACScan flow cytometer.

DNA isolation and PCR analysis. DNA was isolated from brain, thymocytes, and thymic lymphomas using the DNeasy Tissue Kit (Qiagen, Valencia, CA, USA). To determine D-J rearrangement patterns in the *TCRβ* locus, polymerase chain reaction (PCR) was performed as described.[24,25] Of allelic loss analysis at the *Bcl11b* locus, *D12Mit53* and *D12Mit279* markers were used for PCR as described previously.[7] The PCR reaction was processed through 32 cycles of 94°C for 30 s, 55°C for 30 s, and 72°C for 1 min in most cases. The products were analyzed by 8% polyacrylamide gel electrophoresis. PCR bands were stained with ethidium bromide and band intensities were quantitated with a Molecular Imager FX (Bio-Rad Laboratories, Hercules, CA, USA) to determine the allele ratio of BALB/c and MSM alleles or of MSM and BALB/c alleles.

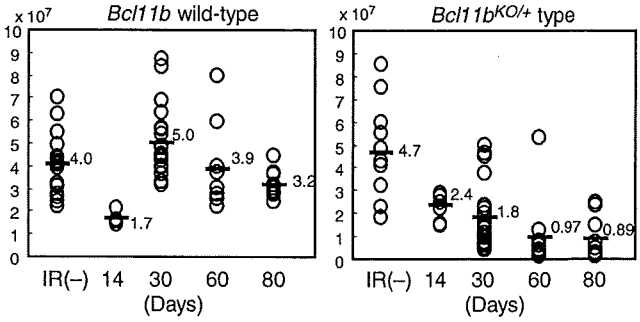

Fig. 1. Cell number in thymuses at various days after γ-irradiation. *Bcl11b*$^{+/+}$ mice, left; *Bcl11b*$^{KO/+}$ mice, right. Average cell number in *Bcl11b*$^{+/+}$ mice was 4.0, 1.7, 5.0, 3.9, and 3.2 × 10^7 cells for unirradiated, 14, 30, 60, and 80 days after irradiation, respectively. Average cell number in *Bcl11b*$^{KO/+}$ mice was 4.7, 2.4, 1.8, 0.97, and 0.89 × 10^7 cells for unirradiated, 14, 30, 60, and 80 days after irradiation, respectively.

Results

Decrease in the thymocyte number in γ-irradiated *Bcl11b*$^{KO/+}$ mice. We subjected 8-week-old *Bcl11b*$^{KO/+}$ and *Bcl11b*$^{+/+}$ mice to 3 Gy of γ-radiation and examined both left and right

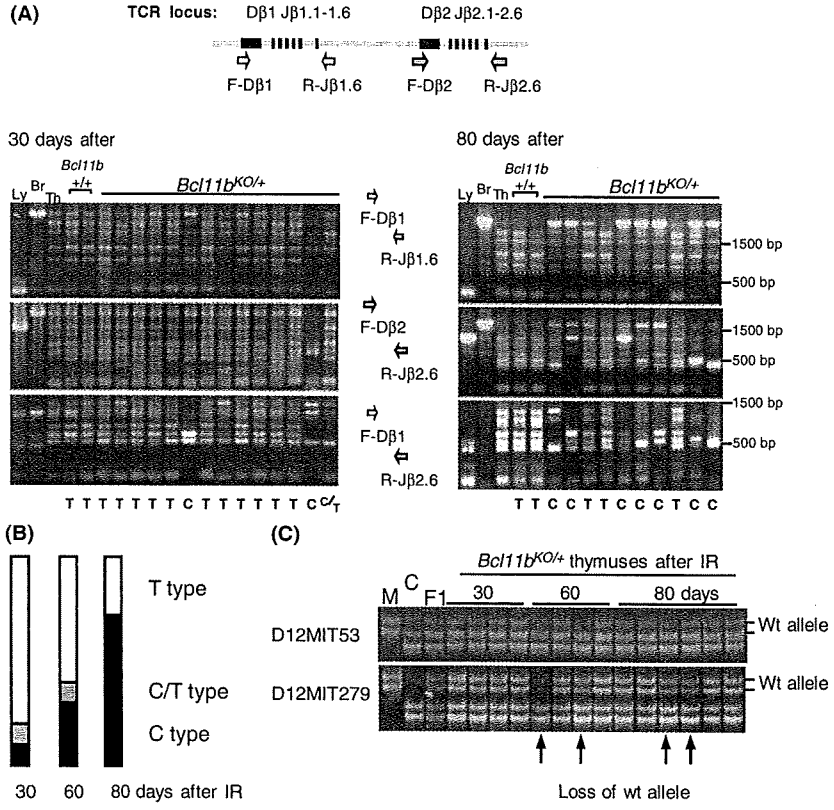

Fig. 2. Clonal growth of thymocytes in thymuses after γ-irradiation of 8-week-old *Bcl11b*$^{KO/+}$ mice. (A) D-J rearrangement patterns at the T cell receptor β-chain (*TCRβ*) locus in thymuses at 30 and 80 days after irradiation. The upper diagram shows part of the *TCRβ* locus and the relative location of PCR primers used. The lower panel shows gel electrophoresis of PCR products with three different sets of primers, F-Dβ1 and R-Jβ1.6 (top), F-Dβ2 and to-Jβ2.6 (middle), and F-Dβ1 and R-Jβ2.6 (bottom). T below the panel indicates T-type thymus that shows identical or similar rearrangement patterns to the control thymus, and C indicates C-type thymus that shows a few bands more prominent than the other bands or limited numbers of bands. C/T indicates C/T-type thymus between the T-type and C-type patterns. Size markers are shown at right. (B) Incidences of C- (black box), C/T- (gray box) and T-type (white box) thymuses in 30, 60, and 80 days after γ-irradiation in *Bcl11b*$^{KO/+}$ mice. (C) Allelic losses at the *Bcl11b* locus in irradiated thymuses. Two panels show polyacrylamide gel electrophoresis for PCR products of *D12Mit53* and *D12Mit279* primer pairs. Chromosomal location of *D12Mit53*, *Bcl11b*, and *D12Mit279* is 108.69, 109.15–24, 109.69 Mb from the centromere, respectively. We determined the allele ratio of BALB/c and MSM bands and judged the thymus as allelic loss-positive when the allele ratio was more than 2 or less than 0.5.

doi: 10.1111/j.1349-7006.2010.01546.x

lobes of the thymus separately at 14, 30, 60, and 80 days after irradiation (the respective thymic lobes are designated as 14-, 30-, 60-, and 80-day thymuses). The earliest time at which fully malignant thymic lymphomas were observed was approximately 100 days after irradiation.[7–9] Figure 1 shows the cell number in the thymuses. In *Bcl11b*$^{+/+}$ mice, the number at 14 days post radiation was not restored to the level in unirradiated mice but restored to the level or more at 30 days after. The cell number was maintained until 80 days after. On the other hand, *Bcl11b*$^{KO/+}$ mice showed impairment in the recovery of cellularity. The cell number at 30 days after was not restored to the normal level in most thymuses and the average was 1.8×10^7 in *Bcl11b*$^{KO/+}$ thymuses which was lower than 5.0×10^7 in *Bcl11b*$^{+/+}$ thymuses ($P < 0.0001$). Also, the cell number was not well maintained at 60 or 80 days after. These results suggest an impairment in the maintenance of thymocyte number in *Bcl11b*$^{KO/+}$ mice after γ-irradiation.

Clonal cell expansion. Clonality was determined by assaying specific V(D)J rearrangements with three primer sets designed for the *TCRβ* locus.[24,25] Figure 2(A) shows PCR patterns of 30- and 80-day thymuses. Unirradiated thymus (lane Th) gave six different bands corresponding to possible recombination sites between D and J regions by Dβ1-Jβ1, Dβ2-Jβ2, and Dβ1-Jβ2 probe sets and one band for germ-line DNA by the former two probe sets. On the other hand, thymic lymphoma DNA (Ly) gave one band only by the Dβ2-Jβ2 probe set used, indicating an identical rearrangement, and brain DNA (Br) gave the germ-line DNA band by Dβ1-Jβ1 and Dβ2-Jβ2 probe sets. Two of the 20 30-day thymuses in *Bcl11b*$^{KO/+}$ mice exhibited only a few bands or limited numbers of bands different from the normal thymus pattern, indicating the existence of clonally expanded thymocytes (C-type thymus). Most others showed rearrangement patterns identical or similar to the control thymus (classified as T-type thymus). There was one thymus that was classified as C/T-type thymus due to the difficulty of distinction between C- and T-type thymus. An additional experiment showed a consistent result, one C/T-type thymus detected in 12 30-day thymuses examined (data not shown). All 20 *Bcl11b*$^{+/+}$ mouse thymuses were T-type thymus (data not shown). On the other hand, the 60-day *Bcl11b*$^{KO/+}$ thymuses showed two C-type and four C/T-type thymuses in 10 thymuses examined, whereas the 80-day *Bcl11b*$^{KO/+}$ thymuses showed six C-type and two C/T-type thymuses in 10 thymuses examined (Fig. 2B). These indicate increase in the incidence of C-type thymus with the time after irradiation. Those results suggest that *Bcl11b*$^{KO/+}$ genotype promotes the development of clonally expanding thymocytes in γ-irradiated mice.

We examined loss of the wild-type *Bcl11b* allele in C- and T-type thymuses using Massachusetts Institute of Technology (MIT) microsatellite markers flanking the *Bcl11b* locus (Fig. 2C). Of the 40 *Bcl11b*$^{KO/+}$ thymuses examined, four exhibited loss of the wild-type allele. All of these were C-type thymus. Their average cell number was as low as 0.20×10^7, and this decrease may be due to a loss of Bcl11b function because *Bcl11b*$^{KO/KO}$ thymocytes exhibit profound apoptosis.[13]

Cell cycle and cell size. We examined the cell cycle distribution of irradiated thymocytes that were isolated from mice at 1 h after intraperitoneal injection of BrdU. We determined the percentage of S-phase cells, size of G1-phase cells, and percentage of a fraction containing large thymocytes in the G1 phase. Figure 3(A) shows examples of flow cytometric analysis. The large cells in the G1 phase (indicated by a horizontal bar) were designated as middle-sized cells because their size was between the size of normal G1 cells (small size) and the size of S phase cells (large size). Figure 3(B) summarizes the percentage of S-phase cells at the vertical axis and the percentage of the middle-sized G1 cells at the horizontal axis in the two groups of 30-day thymuses and 60- plus 80-day thymuses. As for the 30-day thymuses, the percentage of S-phase cells or middle-sized G1 cells did not much differ between *Bcl11b*$^{KO/+}$ and *Bcl11b*$^{+/+}$ thymuses except for one thymus. On the other hand, there were eight *Bcl11b*$^{KO/+}$ thymuses possessing more than 20% middle-sized G1 cells among the 60/80-day *Bcl11b*$^{KO/+}$ thymuses, which were all C type. They showed a considerable variation in the percentage of the S phase. The middle-sized thymocytes may be related with premalignancy because cell-size enlargement is a characteristic of thymic lymphomas.[24] Those thymocytes are probably cells pausing at the G1 stage, and growing and progressing toward the S phase.

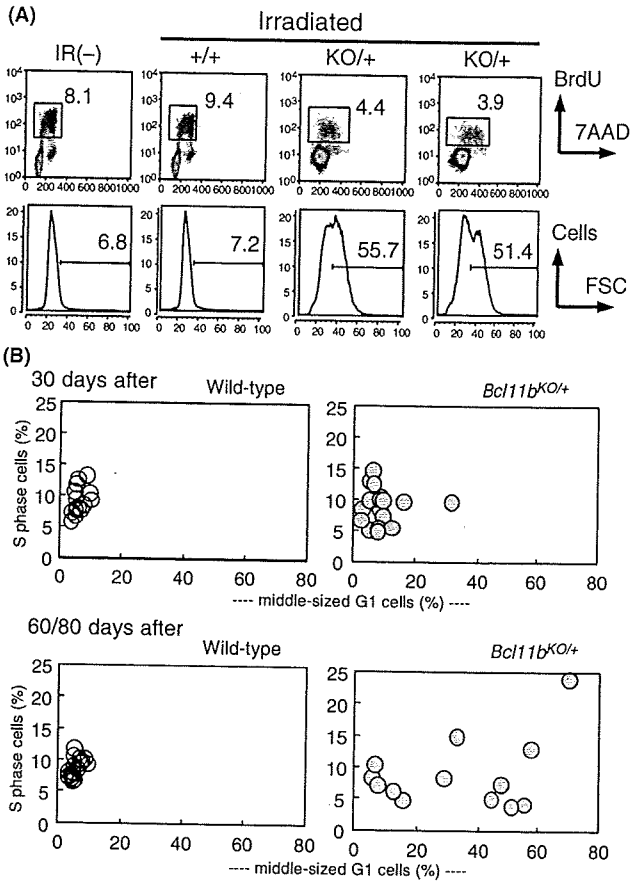

Fig. 3. Cell proliferation and cell size. (A) Flow cytometry of cell cycle in unirradiated and irradiated thymuses. (upper) The vertical axis shows BrdU incorporation levels and the horizontal axis displays 7-AAD staining for DNA contents. A square marks a fraction of thymocytes in the S-phase, and the number gives the percentage of S-phase cells. (lower) The vertical axis shows the cell number and the horizontal axis displays forward scatter (FSC) values reflecting the cell size in G1-phase thymocytes. The bar shows a fraction of thymocytes in large size (middle-sized G1 cells) and the number above the bar indicates the percent of those thymocytes. The percentage was determined in each thymus by the criterion where the percentage in normal thymus was set to approximately 5% of the FSC value. (B) The vertical axis shows the percentage of S-phase cells and the horizontal axis displays the percentage of middle-sized G1 cells. Thirty-day thymuses, upper; groups of 60- and 80-day thymuses, lower; *Bcl11b*$^{+/+}$ thymuses, left; *Bcl11b*$^{KO/+}$ thymuses, right.

Differentiation arrest. Thymocytes from *Bcl11b*$^{KO/KO}$ mice show differentiation arrest at DN and ISP stages to lack DP cells,[13,14] and hence C-type thymocytes or possibly T-type thymocytes may exhibit differentiation arrest. We examined 12 30-day and 10 80-day thymuses with flow cytometry using CD4, CD8, and TCRβ cell surface markers (Fig. 4A,B). We defined

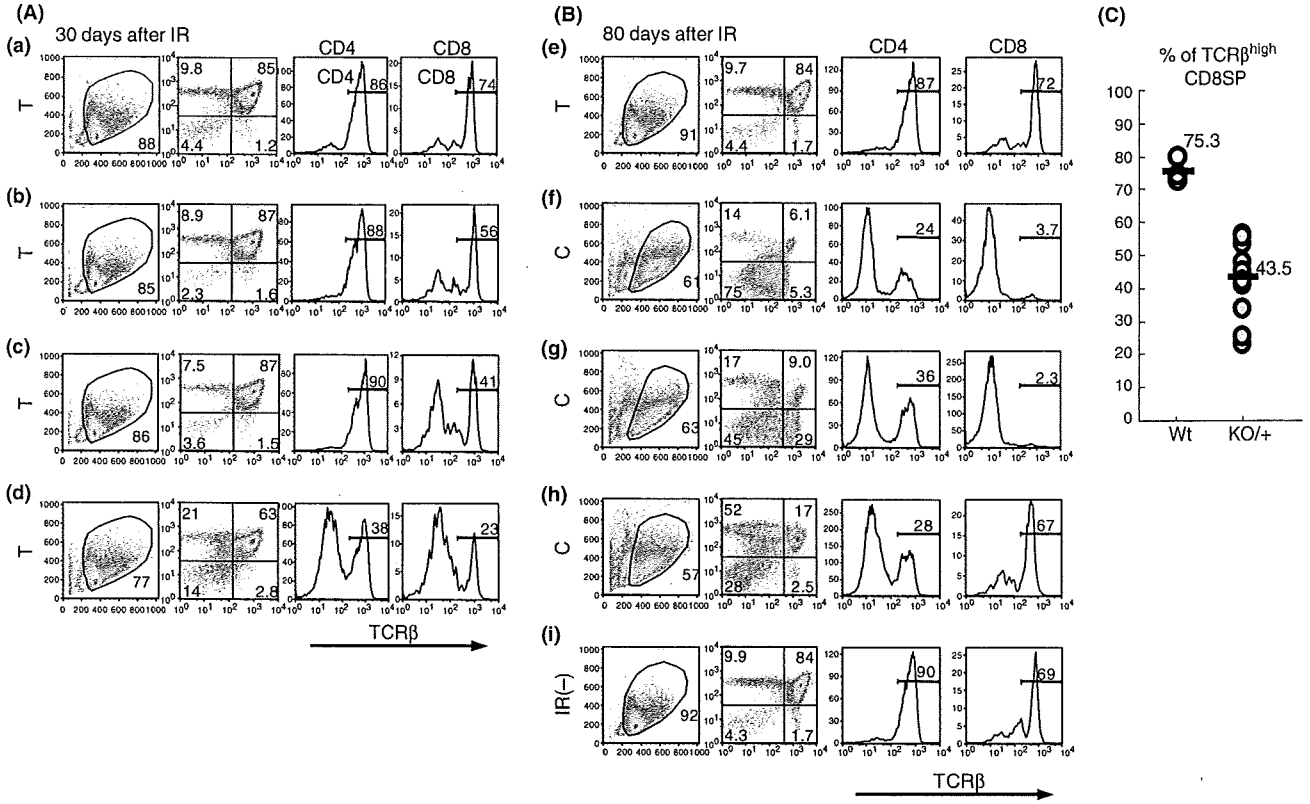

Fig. 4. Flow cytometry of CD4, CD8, and T cell receptor β-chain (*TCRβ*) expression on thymocytes. Thymocytes at 30 days (A) and 80 days (B) after irradiation. (from left to right) The vertical axis shows side scatter (SSC) values and the horizontal axis displays forward scatter (FSC) values (the gated region marked by a circle); the vertical axis shows CD4 expression and the horizontal axis displays CD8 expression; the vertical axis shows cell number and the horizontal axis displays TCRβ expression of thymocytes in the CD4 quadrant; the vertical axis shows cell number and the horizontal axis displays TCRβ expression of thymocytes in the CD8 quadrant. (a) in (A) is a thymus in irradiated *Bcl11b*$^{+/+}$ mice and (b–d) are thymuses in irradiated *Bcl11b*$^{KO/+}$ mice. All four thymuses are T type. (e–h) in (B) are irradiated *Bcl11b*$^{KO/+}$ mice and (i) is an unirradiated *Bcl11b*$^{KO/+}$ mice. (e) is T-type and (f–h) are C-type thymuses. (C) The percentage of TCRβ^{high} CD8SP thymocytes in *Bcl11b*$^{+/+}$ (75.3%) and *Bcl11b*$^{KO/+}$ (43.5%) mice.

the gated region on the FSC *versus* SSC dot plot to exclude debris and dead cells. Although the cell percentage in the gated region did not much differ in the 30-day thymuses, it markedly differed among 80-day thymuses. The fraction of debris and dead cells increased in C- but not in T-type thymuses (data not shown). Analysis of CD4 and CD8 markers revealed that almost all T-type thymocytes of 30-day *Bcl11b*$^{KO/+}$ (also *Bcl11b*$^{+/+}$) mice except for one (d) showed a pattern similar to unirradiated normal thymus, mainly consisting of DP cells. However, analysis of TCRβ showed lower percentages of TCRβ^{high} mature CD8^{+} cells in *Bcl11b*$^{KO/+}$ thymocytes than *Bcl11b*$^{+/+}$ thymocytes (Fig. 4C). These together indicated a small impairment of differentiation in *Bcl11b*$^{KO/+}$ thymocytes. On the other hand, all eight C- and C/T-type thymuses of 80-day *Bcl11b*$^{KO/+}$ mice showed marked differentiation impairment. For instance, (f) in Figure 4(B) shows thymocytes at the DN fraction by CD4 and CD8 expression, and (g) and (h) show thymocytes mainly at the DN/ISP and CD4 fractions, respectively. CD4^{+} SP cells in (h) mostly showed low expression of the TCRβ protein, different from normal CD4^{+} SP cells. These results suggest that the *Bcl11b*$^{KO/+}$ genotype confers differentiation impairment of thymocytes in γ-irradiated mice.

In order to further study the relationship between clonal expansion and differentiation arrest, we subjected 10-week-old *Bcl11b*$^{KO/+}$ mice to 3-Gy γ-radiation and examined thymuses at 30 days after. This experimental condition was chosen based on the higher incidence (6/8, 75%) of C-type thymus observed in mice irradiated at this age and the decrease to 10% (2/20) when mice were irradiated at 4 weeks of age (data not shown). D-J rearrangement assay revealed C-type thymus in six of the 12 thymuses and T-type thymuses in the remaining six (Fig. 5A). The decrease in cell number was observed in *Bcl11b*$^{KO/+}$ mice as predicted, the average number being 1.25×10^{7}. On the other hand, the average of S-phase cells was as low as 4.0% in *Bcl11b*$^{KO/+}$ mice, and there was one C-type thymus possessing more than 20% middle-sized thymocytes. Figure 5(B) shows examples of flow cytometric analysis using CD4, CD8, and TCRβ markers. Of the six C-type thymuses, only two showed differentiation arrest (see b and c), and the remaining four C-type thymuses showed a normal differentiation pattern but lower expression of TCRβ (d and e). This indicated that thymocytes in the four C-type thymuses were capable of differentiating into mature cell types. This contrasts with the results of 80-day thymuses irradiated at 8 weeks of age: all C- and C/T-type thymuses showed impairment in the development of mature thymocytes. These results suggest a process from normally differentiating C-type thymocytes to differentiation-arrested C-type thymocytes in irradiated *Bcl11b*$^{KO/+}$ mice.

Elevation of β-catenin expression in *Bcl11b*$^{KO/+}$ thymocytes. During the flow cytometric analysis using CD4, CD8, and TCRβ markers, we noted a higher percentage of TCRβ^{-} CD8^{+} immature ISP cells and a lower percentage of DN cells in *Bcl11b*$^{KO/+}$ thymocytes (data not shown). The high ISP and low

doi: 10.1111/j.1349-7006.2010.01546.x

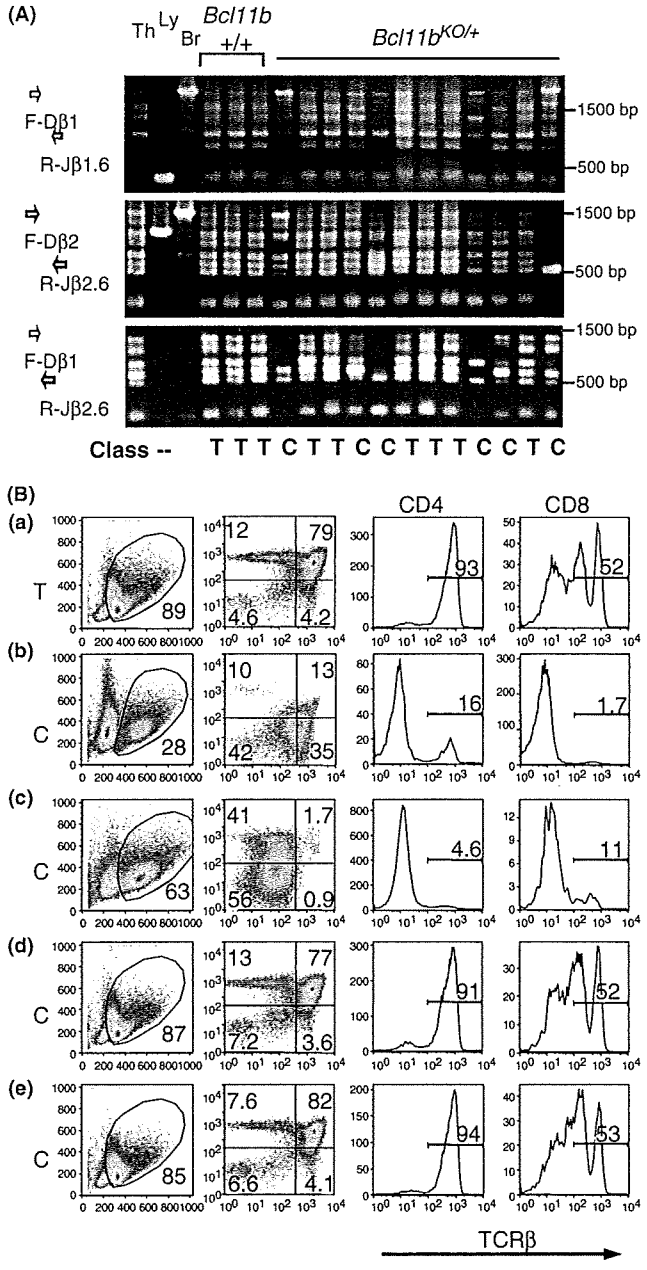

Fig. 5. Analyses of thymuses at 30 days after irradiation of *Bcl11b*$^{KO/+}$ mice at 10 weeks of age. (A) D-J rearrangement patterns at the *TCRβ* locus, as described in the legend for Figure 3(A). (B) Flow cytometry of CD4, CD8, and T cell receptor β-chain (*TCRβ*) expression in thymocytes, as described in the legend for Figure 4. T- or C-type thymus is shown at left.

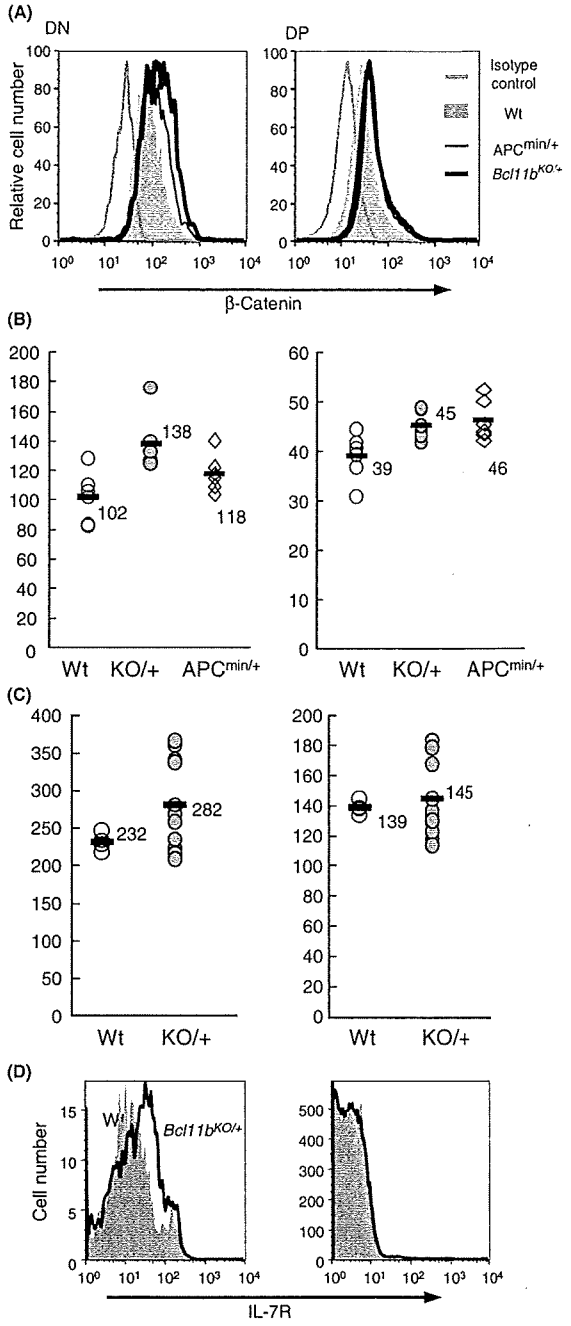

Fig. 6. Flow cytometry of β-catenin and interleukin-7 receptor (IL-7R) expression. (A) β-catenin expression in double-negative (DN) and double-postive (DP) cells of *Bcl11b*$^{+/+}$ (gray region), *Bcl11b*$^{KO/+}$ (bold black line), and *Apc*$^{min/+}$ (thin black line) mouse thymocytes. DN cells, left; DP cells, right. Isotype-matched staining control for *Bcl11b*$^{+/+}$ thymocytes is shown for comparison (gray line). The vertical axis shows relative cell number and the horizontal axis displays β-catenin expression. (B) The mean fluorescence intensity of β-catenin is compared between thymocytes of the three different genotypes. *P*-values in DN and DP cells between *Bcl11b*$^{+/+}$ and *Bcl11b*$^{KO/+}$ mice were 0.0034 and 0.019, respectively. The *P*-value in DP cells between wild-type and *Apc*$^{min/+}$ mice was 0.017. Comparison of the percent of β-catenin-positive cells showed similar results (not shown). (C) Mean fluorescence intensity of β-catenin in thymocytes compared between wild-type (gray circles) and *Bcl11b*$^{KO/+}$ (closed black circles) mice at 30 days after irradiation. (D) IL-7R expression in DN and DP cells of wild-type (gray region) and *Bcl11b*$^{KO/+}$ (black line) mouse thymocytes.

DN percentages, indicative of some differentiation arrest before the DP cell stage, suggested the possibility of an abnormal increase in Wnt/β-catenin signaling.[21–23] Therefore, we examined the expression levels of β-catenin and interleukin-7 receptor (IL-7R), a cell surface receptor downstream from β-catenin signaling.[26,27] Figure 6(A) shows examples of flow cytometric analysis of *Bcl11b*$^{+/+}$ and *Bcl11b*$^{KO/+}$ thymocytes, as well as thymocytes from *Apc*$^{min/+}$ mice as a control. The Apc protein is a component of the degradation complex that modifies and regulates the β-catenin protein level.[23] Consistent with previous reports,[27,28] β-catenin was expressed at higher levels in DN

cells than DP cells in wild-type mice, indicating a down-regulation of β-catenin in DP cells. Figure 6(A,B) shows a comparison of β-catenin levels in DN and DP cells between thymocytes in the three different genotypes. β-Catenin expression was higher in *Bcl11b*$^{KO/+}$ thymocytes in both DN and DP cells and the differences were statistically significant ($P = 0.0034$ and $P = 0.019$, respectively). Elevated β-catenin expression was also observed in the DP cells of *Apc*$^{min/+}$ mice. DN thymocytes of *Bcl11b*$^{+/+}$ and *Bcl11b*$^{KO/+}$ mice at 30 days after irradiation also showed a difference in β-catenin expression (Fig. 6C), suggesting that β-catenin expression was not affected by irradiation. Figure 6(D) shows IL-7R expression at the horizontal axis. Expression of IL-7R in DN cells and its down-regulation in DP cells were also seen, as described previously.[26,27] The IL-7R expression was higher in *Bcl11b*$^{KO/+}$ DN cells than wild-type DN cells, suggesting that IL-7R activation is a reflection of increased β-catenin signaling. These results suggest that elevation of β-catenin activity in *Bcl11b*$^{KO/+}$ thymocytes may affect the proliferation and survival of thymocytes.

Discussion

In this paper we examined γ-ray-induced atrophic thymuses in *Bcl11b*$^{KO/+}$ mice at stages prior to the time of thymic lymphoma development. Clonal expansion of thymocytes, a characteristic of lymphoma cells, was frequently detected in thymuses at 60 or 80 days after 3-Gy γ-irradiation, but at a lower frequency at 30 days after irradiation of 8-week-old mice. On the other hand, it was detected at a high frequency as early as 30 days after irradiation of 10-week-old mice. This age effect on clonal expansion remains to be addressed. Clonal expansion at these early time points was not observed in irradiated mice of the wild-type genotype, but could only be detected when these mice were subjected to 4-times fractionated whole-body γ-irradiation.[25] These results suggest that *Bcl11b* heterozygosity enhances the development of clonally expanding thymocytes and contributes to lymphomagenesis by conferring an effect at an early stage before the start of or during clonal cell proliferation.

Several consequences of *Bcl11b* deficiency have been reported by us and other groups,[13–18] including a loss or decrease of pre-TCR signaling in thymocytes.[14,19] This impairment results in differentiation arrest of thymocytes during β-selection, which may be contributing to lymphomagenesis. The effects of pre-TCR signaling include the stabilization or increased expression of β-catenin via Erk activation that targets several nuclear factors such as early growth response protein (EGR), nuclear factor of activated T-cells (NFAT), and E proteins.[26,27,29–32] Because of the decreased pre-TCR signaling in *Bcl11b*$^{KO/+}$ mice, a decrease in the β-catenin expression was predicted. However, this study demonstrated that β-catenin expression was in fact increased in *Bcl11b*$^{KO/+}$ mice. This increase is another consequence of the *Bcl11b*$^{KO/+}$ genotype, probably independent of the pre-TCR signaling. The expression level of β-catenin is mainly regulated through the modification by a degradation complex consisting of axin, Apc, glycogen synthase kinase 3 (GSK3β), and CDK inhibitor (CKI).[25,33] Although the mechanism is not known, Bcl11b might affect the expression of some of those proteins. We infer that the increase of β-catenin plays a key role in lymphomagenesis, because β-catenin is a well-known oncogenic transcription factor and its stabilization predisposes thymocytes to malignant transformation.[34] β-Catenin targets promoters of *c-myc* and cyclin D1 in a complex with Tcf1 or Lef1, which positively regulate cell cycle progression.[23,33]

Differentiation arrest of thymocytes at the DN or ISP stages was observed in most thymuses that showed clonal expansion. This arrest was not seen in clonally expanded thymocytes induced in *Bcl11b* wild-type mice by fractionated γ-irradiation.[25] Therefore, differentiation arrest may be due to a decrease of Bcl11b function in atrophic thymus. It may be in parallel how the arrest of thymocytes at the DN and ISP stages is a characteristic of *Bcl11b*$^{KO/KO}$ mice.[13] ISP thymocytes in normal thymus are known to be highly proliferative,[35] showing a high percentage of S-phase cells (45% in our experiment; data not shown). However, the ISP cells observed in γ-irradiated thymuses showed low percentages (approximately 5%), suggesting that the thymocytes are phenotypically similar to ISP cells but lack the property of being able to highly proliferate in the thymus. Another finding observed in irradiated *Bcl11b*$^{KO/+}$ mouse thymuses was the decrease in cell number. This may be also ascribed to the decrease of the preTCR signaling that plays a role in survival of thymocytes.[13] On the other hand, there was a group of C-type thymuses with a low cellularity and of a high percentage of middle-sized G1 cells. Those thymocytes of enlarged cell-size might be the prelymphoma cells that have started to form overt thymic lymphomas.

We observed not only thymocytes of clonal origin showing differentiation arrest but also those showing normal differentiation in *Bcl11b*$^{KO/+}$ mice irradiated at 10 weeks of age. The latter thymocytes are a selected clone that already possesses the capacity to self-renew and differentiate into CD4$^+$ and CD8$^+$ SP cells that highly express TCRβ on the cell surface. This kind of thymocyte, possessing the self-renewal and lineage capacity, was also observed in γ-irradiated *Bcl11b* wild-type mice.[25] It may be noteworthy that CML is regarded as a cancer stem cell because of its self-renewal and lineage capacity, fundamental properties for adult tissue stem cells.[6] Though the pathogenesis is distinct between CML and the clonally expanding thymocytes, their similarity in terms of stem cell-like properties may be of interest.[6] It is probable that some of the thymocytes with lineage capacity undergo a change into thymocytes unable to differentiate during lymphoma development. Taken together, the thymocytes possessing self-renewal and differentiation capacities demonstrated in this paper might be related with cancer stem cells or lymphoma-initiating cells. The importance of leukemia-initiating cells is suggested in relapsed ALL in humans because cells responsible for relapse are ancestral to the primary leukemia cells.[36] Of note is that *Bcl11b* may play a role in the formation of lymphoma stem cells in irradiated mice. It remains open, however, what role the stem cell-like aberrant thymocytes play in the development and completion of γ-ray-induced thymic lymphomas and also whether or not such stem cell-like aberrant cells may exist in human *BCL11b*-disrupted T-cell leukemias.[10–12]

In summary, we detected two distinct populations of clonally growing thymocytes in γ-irradiated *Bcl11b*$^{KO/+}$ mouse thymuses. In one population, thymocytes share a common D-J rearrangement but retain the capacity to differentiate. In contrast, thymocytes in the second population have lost their ability to differentiate. Those thymocytes are not fully malignant because of the low cell number, and therefore, the establishment of thymic lymphomas requires an additional change for proliferation to reach completion. The *Bcl11b*$^{KO/+}$ genotype probably influences the clonal expansion and differentiation arrest of thymocytes in γ-irradiated mice and this may be ascribed in part to an increase in the level of β-catenin.

Acknowledgments

We thank Drs Minh To and Yuichi Wakabayashi for critical reading of this manuscript. This work was supported by Grants-in-Aid of Third Term Comprehensive Control Research for Cancer from the Ministry of Health, Labor and Welfare of Japan and for Cancer Research from the Ministry of Education, Science, Technology, Sports, and Culture of Japan.

doi: 10.1111/j.1349-7006.2010.01546.x

References

1 Hanahan D, Weinberg RA. The hallmarks of cancer. *Cell* 2000; **100**: 57–70.
2 Hahn WC, Weinberg RA. Modelling the molecular circuitry of cancer. *Nat Rev Cancer* 2002; **2**: 331–41.
3 Calabretta B, Perrotti D. The biology of CML blast crisis. *Blood* 2004; **103**: 4010–22.
4 Mullighan CG, Goorha S, Radtke I *et al.* Genome-wide analysis of genetic alterations in acute lymphoblastic leukaemia. *Nature* 2007; **446**: 758–64.
5 Mullighan CG, Miller CB, Radtke I *et al.* BCR-ABL1 lymphoblastic leukaemia is characterized by the deletion of Ikaros. *Nature* 2008; **453**: 110–4.
6 Clarke MF, Dick JE, Dirks PB *et al.* Cancer stem cells – perspectives on current status and future directions: AACR Workshop on cancer stem cells. *Cancer Res* 2006; **66**: 9339–44.
7 Wakabayashi Y, Inoue J, Takahashi Y *et al.* Homozygous deletions and point mutations of the Rit1/Bcl11b gene in γ-ray induced mouse thymic lymphomas. *Biochem Biophys Res Commun* 2003; **301**: 598–603.
8 Kominami R, Niwa O. Radiation carcinogenesis in mouse thymic lymphomas. *Cancer Sci* 2006; **97**: 575–81.
9 Kaminura K, Mishim O, Ohi H *et al.* Haploinsufficiency of Bcl11b for suppression of lymphomagenesis and thymocyte development. *Biochem Biophys Res Commun* 2007; **355**: 538–42.
10 Nagel S, Kaufmann M, Drexler HG, MacLeod RA. The cardiac homeobox gene NKX2-5 is deregulated by juxtaposition with BCL11B in pediatric T-ALL cell lines via a novel t(5;14)(q35.1;q32.2). *Cancer Res* 2003; **63**: 5329–34.
11 MacLeod RA, Nagel S, Kaufmann M, Janssen JW, Drexler HG. Activation of HOX11L2 by juxtaposition with 3'-BCL11B in an acute lymphoblastic leukemia cell line (HPB-ALL) with t(5;14)(q35;q32.2). *Genes Chromosomes Cancer* 2003; **37**: 84–91.
12 Przybylski GK, Dik WA, Wanzeck J *et al.* Disruption of the BCL11B gene through inv(14)(q11.2q32.31) results in the expression of BCL11B-TRDC fusion transcripts and is associated with the absence of wild-type BCL11B transcripts in T-ALL. *Leukemia* 2005; **19**: 201–8.
13 Wakabayashi Y, Watanabe H, Inoue J *et al.* Bcl11b is required for differentiation and survival of αβT lymphocytes. *Nat Immunol* 2003; **4**: 533–9.
14 Inoue J, Kanefuji T, Okazuka K, Watanabe H, Mishima Y, Kominami R. Expression of TCRβ partly rescues developmental arrest and apoptosis of αβT cells in Bcl11b-/- mice. *J Immunol* 2006; **176**: 5871–9.
15 Arlotta P, Molyneaux BJ, Chen J, Inoue J, Kominami R, Macklis JD. Neuronal subtype-specific genes that control corticospinal motor neuron development in vivo. *Neuron* 2005; **45**: 207–21.
16 Golonzhka O, Liang X, Messaddeq N *et al.* Dual role of COUP-TF-interacting protein 2 in epidermal homeostasis and permeability barrier formation. *J Invest Dermatol* 2008; **129**: 1459–70.
17 Golonzhka O, Metzger D, Bornert JM *et al.* Ctip2/Bcl11b controls ameloblast formation during mammalian odontogenesis. *Proc Natl Acad Sci USA* 2009; **106**: 4278–83.
18 Avurum Albu DI, Feng D, Bhattacharya D *et al.* BCL11B is required for positive selection and survival of double-positive thymocytes. *J Exp Med* 2007; **204**: 3003–15.
19 Okazuka K, Wakabayashi Y, Kashihara M *et al.* p53 prevents maturation of T cell development to the immature CD4-CD8+ stage in Bcl11b-/- mice. *Biochem Biophys Res Commun* 2005; **328**: 545–9.
20 Fischer A, Malissen B. Natural and engineered disorders of lymphocyte development. *Science* 1998; **280**: 237–43.
21 Gounari F, Aifantis I, Khazaie K *et al.* Somatic activation of beta-catenin bypasses pre-TCR signaling and TCR selection in thymocyte development. *Nat Immunol* 2001; **2**: 863–9.
22 Xu Y, Banerjee D, Huelsken J, Birchmeier W, Sen JM. Deletion of beta-catenin impairs T cell development.Nat Immunol. *Nat Immunol* 2003; **4**: 1177–82.
23 Staal FJ, Clevers HC. Wnt signaling in the thymus. *Curr Opin Immunol* 2003; **15**: 204–8.
24 Ohi H, Mishima Y, Kamimura K, Maruyama M, Sasai K, Kominami R. Multi-step lymphomagenesis deduced from DNA changes in thymic lymphomas and atrophic thymuses at various times after γ-irradiation. *Oncogene* 2007; **26**: 5280–9.
25 Yamamoto T, Morita S, Go R *et al.* Clonally expanding thymocytes having lineage capability in g-ray induced mouse strophic thymus. *Int J Radiat Oncol Biol Phys* (in press).
26 Xu M, Sharma A, Wiest DL, Sen JM. Pre-TCR-induced β-catenin facilitates transversal through β-selection. *J Immunol* 2009; **182**: 751–8.
27 Xu M, Sharma A, Hossain MZ, Wiest DL, Sen JM. Sustained expression of pre-TCR induced beta-catenin in post-beta-selection thymocytes blocks T cell development. *J Immunol* 2009; **182**: 759–65.
28 Weerkamp F, Baert MR, Naber BA *et al.* Wnt signaling in the thymus is regulated by differential expression of intracellular signaling molecules. *Proc Natl Acad Sci USA* 2006; **103**: 3322–6.
29 Carleton M, Haks MC, Smeele SA *et al.* Early growth response transcription factors are required for development of $CD4^-CD8^-$ thymocytes to the $CD4^+CD8^+$ stage. *J Immunol* 2002; **168**: 1649–58.
30 Xi H, Kersh GJ. Early growth response gene 3 regulates thymocyte proliferation during the transition from $CD4^-CD8^-$ to $CD4^+CD8^+$. *J Immunol* 2004; **172**: 964–71.
31 Aifantis I, Gounari F, Scorrano L, Borowski C, von Boehmer H. Constitutive pre-TCR signaling promotes differentiation through Ca^{2+} mobilization and activation of NF-kappaB and NFAT. *Nat Immunol* 2001; **2**: 403–9.
32 Engel I, Murre C. E2A proteins enforce a proliferation checkpoint in developing thymocytes. *EMBO J* 2004; **23**: 202–11.
33 Gregorieff A, Clevers H. Wnt signaling in the intestinal epithelium: from endoderm to cancer. *Genes Dev* 2005; **19**: 877–90.
34 Guo Z, Dose M, Kovalovsky D *et al.* Beta-catenin stabilization stalls the transition from double-positive to single-positive stage and predisposes thymocytes to malignant transformation. *Blood* 2007; **109**: 5463–72.
35 Ioannidis V, Beermann F, Clevers H, Held W. The β-catenin-TCF-1 pathway ensures $CD4^+CD8^+$ thymocyte survival. *Nat Immunol* 2001; **2**: 691–7.
36 Mullighan CG, Phillips LA, Su X *et al.* Genomic analysis of the clonal origins of relapsed acute lymphoblastic leukemia. *Science* 2008; **322**: 1377–80.

平成19年度～21年度 厚生労働科学研究費補助金
第3次対がん総合戦略研究事業 中釜班
総合研究報告書 3／3

疾患モデル動物を用いた環境発がんの初期発生過程及び感受性要因の解明とその臨床応用に関する研究

中釜 斉